Behaviour of Concrete Pavements Exposed to De-icing Salts: Field and Laboratory Studies

By

A.K.M. Rakinul Islam

A Thesis submitted to the Faculty of Graduate Studies of

The University of Manitoba

In partial fulfillment of the requirements of the degree of

Master of Science

Department of Civil Engineering

Faculty of Engineering

University of Manitoba

Winnipeg

Abstract

Concrete pavement deterioration in cold climate regions is a great concern in terms of durability and serviceability perspectives. In particular, the use of different winter road maintenance techniques such as de-icers and anti-icers has been suspected to aggravate the deterioration causing premature joint deterioration. Although, numerous research investigations have been conducted in this area, the root causes and underlying mechanisms behind this deterioration are still not fully understood. Hence, this thesis aims at understanding the role of de-icer salts and identifying possible causes of pavement joint deterioration in the field. Also, it evaluates the performance of concrete containing different supplementary cementitious materials (SCMs) to freezing-thawing cycles in presence of various de-icing salts.

Signs of premature deterioration are customarily observed in areas adjacent to joints in concrete pavements. These areas, especially in cold regions, continue to hold water/solution (due to application of de-icing salts) long after wetting events. This solution can contribute to the deterioration process by physical or chemical mechanisms. In the field study part of this thesis, forensic evaluation was used to classify the source of this damage and identify aspects contributing to joint deterioration of regional (chloride-based salts are directly applied) and residential roads (salts are borne by vehicles tires) in Winnipeg, Canada. In addition to visual inspection, this study characterized the quality of air void parameters and bulk properties (e.g. absorption, penetrability) of cores collected from both regional and residential roads. Also, the alteration of microstructure in concrete was assessed by thermal, mineralogical and microscopy studies. The results revealed that the cores collected from regional roads had high intensity of micro-cracks and most air voids (both small and large) were filled with various levels of secondary depositions compared to the cores collected from residential roads. The deterioration

of concrete is explained by a combination of physical and chemical aspects, due to the interaction of salts, freezing/thawing cycles and wetting/drying with the hydrated paste.

In the laboratory study, novel concrete mixtures incorporating different dosage of fly ash with and without nanoparticles were prepared and subjected to freeze-thaw (F/T) conditions in presence of three different de-icing salts (Sodium Chloride, Magnesium Chloride and Calcium Chloride). Similar mixtures were prepared using General Use (GU) and Portland limestone cement (PLC). The physico-mechanical properties of concrete specimens were assessed during the exposure period. Also, the alteration of microstructure in concrete was assessed by thermal, mineralogical and microscopy studies. At the end of 600 F/T cycles, all the nano-modified concrete specimens were intact and able to resist this aggressive exposure. Comparatively, the reference GU specimens (without any SCMs) suffered physical and chemical deterioration in the calcium chloride and magnesium chloride salt solutions. The performance of PLC concrete specimens was comparable and in some instances, better in comparison to the corresponding GU specimens.

Dedication

I would like to dedicate this thesis to my beloved parents whose unconditional love, support, guidance and prayers helped me to come this far.

Acknowledgements

[In the name of most wise and merciful Allah (sbw)]

I cannot be thankful enough for all the countless blessings and mercy that my creator almighty Allah (sbw) has showered upon me. Specially I am ever grateful to be blessed with the opportunity to pursue my higher studies at University of Manitoba in a renowned research group in the field of structural materials and durability. It was a privilege and honor to work under the guidance of Dr. M T Bassuoni, P.Eng., Associate Professor, Department of Civil Engineering, University of Manitobawho not only shared his wisdom but also provided a constant support to successfully accomplish the goals of this research work. Therefore, my most sincere gratitude goes to my supervisor Dr. M T Bassuoni. I would also like to acknowledge all the technical support and valuable guidance of all my colleagues specially Ahmed Ghazy for being an excellent mentor and a great critique of my work.

I do sincerely thanks Mr. Chad Klowak, P.Eng.,W.R.McQuade Heavy Structures Laboratory Manager, University of Manitoba for all his technical support and IKO materials testing facility. Last but certainly not the least, I thank my parents whose constant support, proper guidance and faith helped me to overcome all the obstacles and achieve success in pursuing my higher studies.

Table of Contents

List of Tables

List of Figures

Abbreviation/Nomenclature

CH- Calcium hydroxide

C-S-H- Calcium silicate hydrate

EDX- Energy Dispersive X-ray analysis

F/T- Freezing and thawing

GU- General use

ITZ- Interficial transition zone

MIP- Mercury Intrusion Porosimetry

M-S-H- Magnesium silicate hydrate

PLC- Portland limestone cement

RCPT- Rapid Chloride Penetrability Test

RE_d - Relative dynamic modulus of elasticity

SCMs - Supplementary cementitious materials

SEM- Scanning Electron Microscope

W/T- wetting and drying

XRD- X-ray Diffraction

1. Introduction

1.1. Overview

Road network systems are an integral part of modern development. Due to the cost, availability, maintenance and many other related factors concrete is one of the most preferred material over the years for transportation infrastructure. However, maintaining pavement serviceability in harshly cold regions remains a challenging task. Many government agencies in North America and Europe expect service life of concrete pavements to be in the range of 30 to 50 years (American Concrete Pavement Association 2002; Hall et al. 2007; Holt et al. 2011). Whereas many of these pavements provide excellent long-term performance, a portion of these pavements recently has shown premature deterioration. This deterioration is considered problematic because it compromises the performance and potential service life of an otherwise sound pavement, thus impairing the ride quality. This is a great concern to transportation agencies, which are spending a considerable expenditures for repairing deteriorating pavement sections.

1.2. Deterioration of Concrete Pavement

Concrete pavements premature joint deterioration has been identified at different places in North America. Signs of this deterioration is shown at or near the longitudinal and transverse joint areas. Cracking and spalling accompanied by loss of concrete material adjacent to the joint areas are the main features of this deterioration. In addition, hollow bulb shaped damaged zone underneath the sealed joint areas have also been identified. Until now, the root causes behind joint deterioration are not fully understood since a multitude of reactions and mechanisms are responsible for this deterioration (de-icing salts, freezing-thawing [F/T] and wetting-drying [W/D] cycles, degree of saturation, etc.). Previous in-situ evaluations (Rangaraju 2002; Arribas-

Colón et al., 2012; Kang et al., 2012; Jain et al., 2012) in multiple sites revealed that, in many cases, the joints continued to hold water/solution (due to application of de-icing salts) long after wetting events. This solution is involved in the deterioration by physical actions (generation of micro- and macro-cracks by increasing the degree of saturation) or chemical reactions (leaching/decomposition of hydration products and formation of expansive phases) (Kang et al., 2012; Jain et al., 2012). It has been suspected that the widespread use of specific types of de-icing salts may have played a role in either triggering or accelerating the concrete pavement distress (Jain et al., 2012, Mori et al., 2013, Peterson et al., 2013, Wu et al., 2014). Also, changes in de-icing practices such as implementation of anti-icing (to prevent the bonding of ice to the roadway before a storm) and de-icing strategies (to melt and break down the bond between the ice layer and the road surface) may impart deleterious effects on concrete pavements and reduce its integrity and durability.

Various laboratory simulation studies have adopted different exposure schemes to imitate the conditions experienced by concrete pavements. Previous laboratory studies (Santagata and Collepardi, 2000; Sutter et al., 2006; Wang et al., 2006; Darwin et al., 2008; Jain et al., 2011; Shi et al., 2011; Peterson et al., 2013; Wu et al., 2014; Farnam et al., 2015) have showed that, the effect of de-icing salt vary significantly depending on the type and concentration of de-icing salts. Not only physical but also chemical deterioration play significant role in concrete damage. Combined effect of physical and chemical deterioration is more detrimental to concrete than their individual effects.

1.3. Introduction of Novel and Supplementary Materials in Concrete Pavements

Incorporation of supplementary cementitious materials (SCMs) specially Class F fly ash (low calcium oxide) with cement showed promising improvements in concrete durability

characteristics. However, the slow strength gain and vulnerability to surface scaling kept the use of fly ash in concrete pavement construction limited and optional. For instance, surface works specifications in Manitoba (2014) mandate that the use of fly ash as a cement replacement in concrete pavements, curbs, sidewalks, etc. is optional, and if used, it must not exceed 15% (Public Work Department, City of Winnipeg, 2014).

Research has shown that, addition of nanoparticles can vigorously speed-up the kinetics of cement hydration and efficiently refine the pore structure of concrete (Sanchez et al., 2010). Said et al.(2012) reported that incorporation of nanosilica with 30% class F fly ash can improve concrete microstructure and reduce the portlandite/calcium hydroxide (CH) content in cementitious system within 28 days. As portlandite is among the main reactants with de-icing salts in the chemical deterioration process of concrete pavements (Sutter et al., 2006; Jain et al., 2011; Shi et al., 2011; Peterson et al., 2013), limited production of portlandite is beneficial for concrete deterioration. Thus, the nanoparticles incorporated with SCM in concrete pavement construction may have a great potential to provide durable concrete with long term performance.

On the other hand, portland limestone cement (PLC; portland cement comprising up 15% inter-ground limestone filler with clinker) has been used in Europe (European Committee for Standardization (CEN) Standard EN 197-1) and recently introduced in Canada (CSA A3000-13) and USA (ASTM C150/C150M-16 and ASTM C1157/C1157-14). It was applied in few demonstration projects of concrete pavements (e.g. Thomas *et al.*, 2014). Introduction of PLC in North American market has been made to reduce the CO_2 emission associated with the production of Portland cement. However, lack of long-term performance and research data in cold environments might prove risky in terms of durability and performance of PLC in pavement construction.

1.4. Need for Research

Several premature joint deteriorations and focus studies (Yang et al., 2011, Taylor P.C., 2011, Kang et al., 2012, Arribas-Colón et al., 2012, and Panchmatia et al., 2014) have been reported. However, the mechanisms of damages are not yet fully understood. Structural design (e.g. joint spacing, saw-cutting window and depth, drainage system), construction practices (e.g. addition of excessive amounts of water during placement, vibration rates, improper curing), harsh service conditions (e.g. de-icing salts, freeze-thaw [F/T] cycles, wet-dry [W/D] cycles) and properties of concrete (e.g. penetrability, air-void quality) have been broadly linked to joint deterioration of concrete pavements. The problem is common enough in cold climate regions that focused work on the deteriorated concrete pavement joints from the streets and roads in Winnipeg is needed to investigate the underlying causes of premature joint deterioration.

Presence of chloride based de-icing salts impart deleterious effects on concrete pavement and reduce its integrity and durability. Considering this fact, extensive research works (Cody et al., 1996; Marchand et al., 1999; Lee et al., 2000; Wang et al., 2006; Shi et al., 2010; Jain et al., 2012; Mori et al., 2013; Wu et al., 2014) have been conducted to investigate concrete deterioration in presence of different de-icing salts. However, very few studies considered salt concentrations based on phase diagrams where the chloride ion concentration is equal for all salt solutions used. On the other hand, the long-term serviceability and durability of concrete can be Improved by the incorporation of SCMs such as Class F fly ash. Despite having these benefit the use of fly ash in roadway construction is optional and limited by small dosages. Research showed that addition of nanoparticles with fly ash can produce concrete with superior quality. Therefore, to introduce the use of nano-modified fly ash concrete in pavement construction, its performance is required to be evaluated through research. Furthermore, with the absence of long-

term field performance and robust research data, the application of PLC in transportation infrastructure exposed to chloride based de-icing salts might be risky. Hence, extensive research is still needed for comparative performance of PLC and general use (GU) cement based concrete in extreme exposure conditions.

1.5. Objectives

The primary objectives of this thesis are to:

- Characterize and investigation of the possible causes of premature joint deterioration of field concrete pavement.
- Evaluate the performance in terms of physio-mechanical properties and microstructural features of nanomodified fly ash concrete in presence of various de-icing salts and F/T conditions.
- Compare the performance of GU and PLC cement concrete in extreme exposure conditions (F/T cycles) with chloride based de-icing salt solutions.

1.6. Scope of Work

To achieve the afore mentioned objectives, the research work was divided in two phases. The first phase consisted of the investigation and analysis of collected cores from concrete pavement in Winnipeg. The second phase comprised the laboratory simulation work which evaluated the performance of novel concrete mixtures in the presence of various chloride based de-icing salts and F/T cycles.

Field study: To develop a better understanding of premature joint deterioration mechanisms, cores collected from different street zones of Winnipeg were examined. The changes in bulk properties, microstructure and chemistry of concrete cores were evaluated. A series of macro-

and micro-scale tests were conducted to evaluate the nature of the distress. A systematic study was carried out; A total of 48 cores were taken at multiple locations to capture the effect of different winter treatments in the pavement sections under investigation. The fluid transport properties and physical resistance of the collected cores were examined through Absorption, Rapid Chloride Penetrability Test (RCPT) and Mercury Intrusion Porosimetry (MIP) test. To assess the condition and effectiveness of air void system in collected cores an automated flatbed scanner method was applied. To identify the alteration of microstructure in deteriorated cores thermal and mineralogical analyses were carried out.

Laboratory study: To provide guidance to produce durable concrete for concrete pavement in cold climate regions, a wide range of concrete mixtures containing GU cement and PLC were produced. The mix designs were produced using two dosages (20% and 30%) of fly ash without and with nanoparticles (nanosilica). All the concrete mixtures were subjected to F/T conditions and three types of de-icing salts (NaCl, $MgCl_2$, and $CaCl_2$). To evaluate the performance of the specimens, visual observation, expansion and mass change were determined. Relative dynamic modulus of elasticity measurements was also made regularly to identify internal damage. The underlying mechanisms of damage and alteration of microstructure in deteriorated specimens were investigated by microscopy, thermal and mineralogical analyses.

1.7. Thesis Structure

The thesis is divided into six chapter:

Chapter one contains introduction, overview, deterioration of concrete pavement, introduction of novel and supplementary materials in concrete, research objectives and scope of work.

Chapter two presents a brief literature review of concrete pavement deterioration. This includes a discussion on various damage mechanisms of concrete pavement along with various durability issues. The deleterious effects of de-icing salts on pavement deterioration were discussed with the physical and chemical damage aspects. Previous studies on field concrete and laboratory specimens were also presented.

Chapter three describes the methodology, materials, and mixtures used in the test program. It also elucidates different salt solutions prepared based on the phase diagram of salts for the F/T exposure, physico-mechanical properties and microstructural, mineralogical and thermal analyses.

Chapter four presents the results and discussion for the field study conducted on collected pavement cores from various streets in Winnipeg. Physical penetrability, air void parameters and microstructural analyses were made to shed light on the pavement joint deterioration mechanisms and effect of de-icing salts.

Chapter five includes test results and discussion on F/T exposure of nano-modified fly ash concrete mixtures. It explains the effects of nanosilica and various dosages of fly ash in concrete to withstand F/T conditions in presence of various chloride based de-icing salts.

Chapter six provides a summary of the research program, concluding remarks based on the test results and recommendations for future research.

2. LITERATURE REVIEW

2.1. Introduction

Previous research investigations identified different damage mechanisms which can lead to different pavement deteriorations. This literature review focuses on the effects of various de-icer and anti-icer salts on concrete pavement distress. Previous laboratory and field investigations are also presented here.

2.2. General Damage Mechanisms of Concrete Pavements

The road transportation facility, in North America, is basically based on concrete infrastructures (roads, highways, bridges, parking lots etc.). According to Public Works Canada, approximately 12 billion dollars are spent annually on pavements in Canada. The areas which experience larger extreme in temperature especially during winter are more susceptible to various kinds of pavement distress. In addition to harsh cold climate, extensive use of de-icer and anti-icer salts also aggravate the deterioration of concrete pavements. Recently, premature pavement joint deterioration has been reported which typically is the cracking and spalling of concrete along with the loss of material from joint areas. The reason behind that is not well-understood but various actions and factors such as freezing-thawing (F/T), wetting-drying (W/D), de-icer chemical effect, degree of saturation, D-cracking etc. have been reported to be responsible for this problem. Yet, no one mechanism is identified to fully explain this deterioration process.

The general damage mechanisms of different pavement deteriorations are highlighted in the following subsections.

2.2.1. Scaling

Scaling damage refers to the progressive removal of small chips or flakes from the surface of concrete pavement. Concrete exposed to freezing and thawing in presence of de-icer salts encounter this superficial damage which results in accelerated water and ion ingress. Scaling increases the susceptibility of concrete pavement to high degree of saturation, thus, makes it more vulnerable to further damage and more durability issues related to pavements. (Valenza and Scherer, 2007; Yener and Hinislioglu, 2011).

2.2.2. D-cracking

D-cracking is a progressive distress in concrete pavement generally associated with coarse aggregate in concrete pavement. Use of non-frost resisting coarse aggregate propagates D-cracking because of its inability to withstand F/T action. Concrete which is critically saturated by moisture penetration through cracks and joints subjected to repeated F/T exhibit the signs of D-cracking (Schwartz, 1987). Generally, it is found initially at the intersection of longitudinal and transverse joint sections and lately at transverse cracks. The cracking starts at the corner areas and then proceeds along the joints. Moreover, D-cracking generally initiates at the base of the pavement and progresses upward with time (Koubaa and Snyder, 2001). It becomes visible at the pavement surface as a series of small cracks often accompanied by discoloration of the affected portion. D-cracking weakens the concrete and may eventually lead to its disintegration near the joint areas. Figure 2.1 shows the D-cracking problem at a pavement joint.

Figure 2.1: D-cracking of concrete pavement.

2.2.3. Blowup

The shattering or upward buckling of a concrete pavement at pavement joints or cracks is known as "blowup". Blowups usually occur at the transverse joints or cracks when enough space is not allocated for the expansion of slab (Shahin, 2005). Axial compression force on concrete, induced by the rising temperature and moisture, builds excessive pressure and expansion which forces the concrete pavement to buckle or crumble along the transverse joint (Kerr and Dallis, 1985; Sargious, 1975).

2.2.4. Cracks: longitudinal, transverse and diagonal

Transverse, longitudinal and diagonal cracks divide the concrete slab into two or more pieces. Combination of repeated loading, curling and drying shrinkage helps to develop transverse and diagonal cracks in concrete pavements. The longitudinal cracks are the result of load repetition, weak road bed support and induced warping by temperature and moisture gradient (Bautista and Basheer, 2008; Shahin, 2005). Figure 2.2 shows different types of cracking.

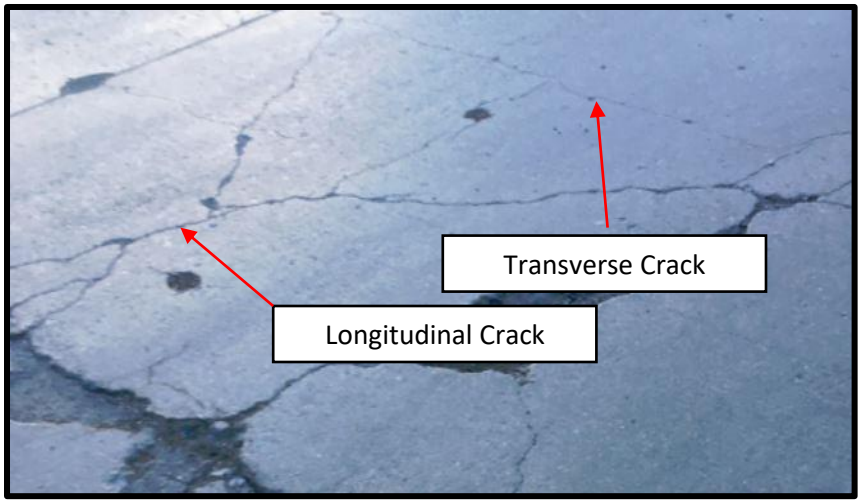

Figure 2.2: Longitudinal and transverse cracks.

2.2.5. Pumping

Pumping is one of the major causes of failure of rigid pavement where water along subgrade materials is expelled through the joints, cracks and edges when subjected to heavy loading. The plastic deformation of subgrade materials and voids beneath pavement slab due to curling or warping allows the accumulation of water inside the slab (Bhatti et al., 1996). The continuous action of pumping results in redistribution of subgrade material and formation of larger voids beneath the slab which lead to more deformations and premature cracking of concrete pavement (Van Wijk et al., 1989; Bhatti et al., 1996).

2.2.6. Pop-outs

Pop-outs are a form of concrete distress that can be triggered by the expansive and nondurable aggregate and can be initiated by the F/T action. When water freezes in pores of coarse aggregate near the surface, it forces the aggregate to expand and eventually small flakes of concrete from the surface comes out or spall off. Alkali-Silica Reactivity (ASR) can also cause pop-out distress

where small parts of concrete break away from the surface of concrete pavement (Bautista and Basheer, 2008). Figure 2.3 represents the pop-out distress of concrete pavement.

Figure 2.3: Pop-out at concrete surface.

2.2.7. Faulting

Faulting is a vertical displacement of concrete slab at transverse joints which indicates the potential failure of the joint. The base material beneath the transverse joint containing considerable amount of fine materials, combined with water, results in faulting when experiencing heavy loading (Bautista and Basheer, 2008).

2.2.8. Polishing

Surface polishing is the loss of skid resistance of pavement as a result of losing surface texture. This distress mechanism is caused by friction between traffic tires and pavement surface. Also, it may also be attributed to the use of soft aggregate in the construction of the pavement (Bautista and Basheer, 2008).

2.2.9. Joint or crack spalling and joint seal damage

Joint or crack spalling refers to the loss of concrete from the edges of joints or cracks of concrete pavement and continuous widening of the cracks which eventually lead to the disintegration of

cracked edges. An accelerated slab failure may occur if crack spalling occurs due to the movement of two individual slabs against each other during the events of repeated heavy loading (Bautista and Basheer, 2008). Under traffic load, the micro cracking caused by the improper joint action known as 'Chattering Action' may lead to early-age minor spalling (Detwiler et al., 2001). In a joint seal damage, accumulation of incompressible materials such as soil or rocks in the joint allows water to infiltrate inside and prevents the slabs to expand which may result in buckling, spalling or shattering of concrete pavement (Shahin, 2005). Joint spalling in concrete pavement is shown in Figure 2.4

Figure 2.4: Joint Spalling

2.2.10. Curling and warping

The temperature and moisture gradient in concrete pavement instigate the curling and warping in a rigid pavement. The difference of moisture content at various depths in a concrete slab forces the concrete to warp towards the drier region due to shrinkage (Bianchini, 2013; Fang, 2001). The drying shrinkage due to moisture gradient results in a curling moment in the slab that in turn causes the uplifting of corners and edges of the slab. A concrete pavement undergoes the

warping event on a daily basis where the effect of warping is higher at night due to increased moisture gradient and reduced temperature gradient (Rao and Roesler, 2005; Fang, 2001).

2.2.11. Map crazing/cracking

Map crazing or map cracking is the hairline cracks appearing on the surface of a concrete pavement (Figure 2.5). It is a network of shallow depth cracks usually occur by over finishing but can also be induced by the alkali-aggregate reaction. Map cracking can lead to the surface scaling and make concrete vulnerable to more durability issues (Shahin, 2005).

Figure 2.5: Map crazing/ cracking

2.2.12. Corner cracking

Corner cracking is a diagonal crack which connects with a longitudinal and transverse crack and intersects joints creating a triangle (Shahin, 2005; Sargious, 1975). It can cause the breakup of slabs while experiencing traffic load on unsupported corners, weak subbase and warped or curled rigid pavements (Bautista and Basheer, 2008; Sargious, 1975).

2.3. Durability Issues with Concrete Pavements

The durability of concrete pavement is often compromised by different reactions and mechanisms such as F/T damage, W/D damage, alkali-aggregate reaction (AAR), alkali-silica reaction (ASR), sulfate attack etc. All these degradation processes initiate with the presence of

water and aggressive ions e.g. chlorides and sulfates. Water containing these harmful ions penetrates into concrete pore structure and causes damage while leaving behind a concrete with reduced integrity and strength that is susceptible to further damage. Thus, the extensive use of chloride based deicing and anti-icing salts poses great potential for detrimental effects and durability concerns to concrete infrastructures (Sutter et al., 2006; Wang et al., 2006; Shi et al., 2010, 2011; Jain et al., 2011; Peterson et al., 2013).

In winter seasons, to alleviate road hazards and maintain the functionality, salting is the most popular method that is widely used by government agencies. De-icing and anti-icing are the two methods followed for the application of road salts during winter road maintenance. The de-icing and anti-icing are distinguished by the time of application of salts on road surface (Sutter et al., 2008, Hossain et al., 2014). In de-icing technique, the salts or chemicals (e.g. magnesium chloride, calcium chloride, calcium chloride etc.) are applied after the snowing event to lessen the bond between the accumulated ice and road surface. On the contrary, anti-icing is the application of salts or chemicals before the event of snowfall and can be defined as the proactive use of any de-icer. In this case, wetting of road surface with salt solution hinders the bonding of ice and concrete pavement (Kelting et al., 2010). However, these de-icers and anti-icers can instigate various durability issues in concrete pavements through both physical deterioration and chemical reactions (Santagata and Collepardi, 2000; Sutter et al., 2006; Wang et al., 2006; Darwin et al., 2008; Valenza et al., 2007; Shi et al., 2010,2011; Jain et al., 2011; Peterson et al., 2013). The following sections depict the characteristics of de-icers and anti-icers and their detrimental effects on concrete pavements.

2.4. Characteristics of Commonly Used De-icer/Anti-icer Salts

Road salts are not only very effective in breaking the bond between the ice and pavement surface but also have snow and ice melting capacity, low price and easy accessibility. Therefore, application of salts, as a de-icer and anti-icer, is the most common method of snow and ice control in roads and highways. Among all, sodium chloride (NaCl) salt is the most widely used de-icer/anti-icer by various governmental agencies. However, the efficiency of snow and ice melting capacity of NaCl is reduced drastically below 18°F (-8°C) (Jain et al., 2012). As a consequence, at lower temperatures, salts with higher ice melting capacity such as calcium chloride ($CaCl_2$) and magnesium chloride ($MgCl_2$) are increasingly used in winter pavement control operations (Sutter et al., 2008; Jain et al., 2011,2012).

The theoretical melting capacities of all de-icing salts are characterized by its eutectic curve (Figure 2.6). Each de-icer salt has its own eutectic temperature. To determine the target concentration for de-icer solution, the eutectic temperature is used as a guideline. The eutectic temperature refers to the lowest point at which solution can remain in a liquid phase and directly borders with the solid phase. According to this binary de-icer-water phase diagram, this is the lowest temperature at which a de-icer can melt ice or snow. The general pattern of the curved line demonstrates a higher amount of solute is required at lower temperatures to melt the ice until the eutectic temperature is reached (Darwin et al., 2008; Kelting et al., 2010). As temperature declines, the chemical potential of ice also goes down; therefore, a higher concentration of solute is needed to achieve the required chemical gradient to melt ice at lower temperatures. However, presence of $Ca(OH)_2$ from cementitious matrix in concrete alters the behaviour of conventional binary phase diagram (e.g. $CaCl_2$-H_2O), thus the eutectic temperature does not provide a reliable

forecast of effective temperature range for the de-icer chemical to melt the snow and ice (Farnam et al., 2015).

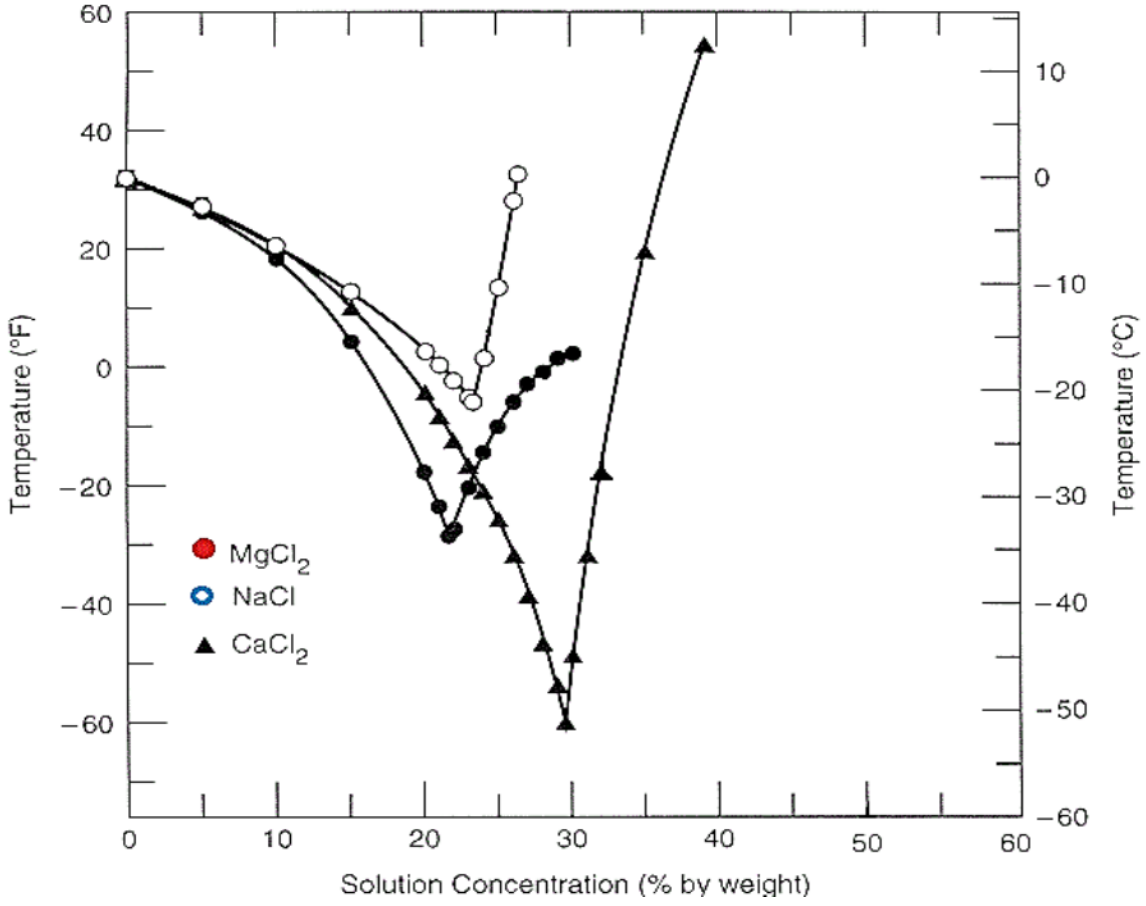

Figure 2.6: Phase diagrams of various de-icer salts (adapted from Kelting et al., 2010)

2.5. De-icer/Anti-icer Effect on Concrete

De-icers affect concrete both physically and chemically (Sutter et al., 2006; Wang et al., 2006; Darwin et al., 2008; Valenza et al., 2007; Shi et al., 2010,2011; Jain et al., 2011; Peterson et al., 2013). The physical damage from de-icer salt on concrete pavement is the intensified freezing and thawing distress typically manifested as salt scaling and cracking along with concrete degradation and premature failure especially in joint areas. On the contrary, chemical effect is the result of various detrimental reactions involved with de-icers, cement hydration products,

aggregates and corrosion reaction where reinforcement steel exists. Presence of alkalis in de-icer chemical can initiate and accelerate the alkali-silica reaction and alkali-carbonate reaction, while critical concentration of chloride ion accumulated at the vicinity of reinforcement steel, present in concrete, can initiate corrosion (Hoffmann, 1984; Nixon et al., 1988; Brown and Doerr, 2000; Shi et al., 2010). Some researchers emphasized that the combined effect of physical and chemical action results in more damage in concrete than their separate actions (Wang et al., 2006; Li et al., 2011). Previous studies on the effect of de-icers (Cody et al., 1996; Lee et al., 2000; Sutter et al., 2006, Wang et al., 2006; Darwin et al., 2008) indicate that the de-icer's impact on concrete pavement differs based on salt concentration, exposure condition and test temperature.

2.5.1. Physical damage mechanisms of concrete pavements

Physical damage in concrete pavement can be initiated by various processes such as concrete exposure to F/T cycles with a high degree of saturation, production of internal stress due to salt crystallization, expansive forces due to the initiation of reinforcement steel corrosion, and lastly the scaling of concrete surface (Marchand et al., 1994; Valenza et al., 2005; Li et al., 2011; Farnam et al., 2015). The presence of deicing salt often exacerbates the surface scaling during F/T events by creating pressure through hydraulic, osmosis, and crystallization process. In addition to creating pressure, deicing chemicals accelerate the degree of saturation in concrete pores and increase the risk of frost damage (Litvan, 1976; Harnic et al., 1980).

Extensive research work has been done to identify the mechanisms behind the de-icer and F/T related deterioration. A number of mechanisms have been proposed as the root cause behind these deteriorations. However, no specific mechanism has been found yet to be solely accounted

for salt scaling effect. This might be a result of combined effect of several mechanisms. The description of these mechanisms is indicated in the following subsections.

2.5.1.1. Hydraulic pressure theory

One of the major damage mechanisms in concrete due to F/T action is related to the hydraulic pressure and ice expansion. During freezing, water starts to freeze inside the larger capillary pores first. The formation of ice causes volume increase by 9% and results in extra water to force out from the capillary pores. This expelled water generates the hydraulic pressure in concrete. The magnitude of the induced hydraulic pressure is dependent on the rate of freezing, degree of saturation and expelled water flow path (Powers and Helmuth, 1953; Setzer, 2001). When the hydraulic pressure in concrete surpasses the tensile strength of concrete, cracking of concrete takes place. Air entrainment and void spacing plays a vital part to resist the hydraulic pressure effect and delays the critical degree of saturation in concrete (Powers and Willis, 1950).

2.5.1.2. Osmotic pressure theory:

Powers and Helmuth (1953) proposed the Osmotic pressure theory where water is diffused towards the ice in capillary pores from the gel pores. At or below the freezing temperature, water in capillary pores turn into ice and the difference in entropy forces the unfrozen gel water to diffuse towards the frozen ice causing the fluid pressure to rise (Powers and Helmuth, 1953). Diffusion of pore water increases the growth of ice bodies and generates the osmotic pressure. The pore walls in concrete experience a tensile stress resulting from the created osmotic pressure. The osmotic pressure is initially started by the generation of hydraulic pressure in concrete pores and the concrete may deteriorate by the combined effect of both the hydraulic and osmotic pressure (Valenza and Scherer, 2006; Rosli and Harnik, 1980).

2.5.1.3. Crystallization pressure

Formation and growth of salt crystals create tensile stress in the concrete porous skeleton and due to these crystal formations, the generated crystallization pressure plays the major role in the frost damage of concrete (Helmuth, 1960; Valenza and Scherer, 2007). Precipitation of salt crystals, due to higher salt ion concentration inside the capillary pores than the concrete surface, can cause severe damage. Growth of salt crystal happens always towards the pore wall which generates the crystallization pressure and tries to push the pore wall away with a force dependant on the curvature of the crystal. Supersaturation of pore liquid is the pre-requisite for the generation of high crystallization pressure. Damage caused by crystallization pressure depends on supersaturation ratio, pore size, and the magnitude of repulsive force between the salt crystal and the confining pore surface (Thaulow and Sadananda, 2004; Scherer, 2004; Valenza and Scherer, 2007; Wardeh et al., 2011)

2.5.1.4. Super-cooling

Presence of de-icer salt suppresses the ice formation in concrete pores and water freezes at a lower temperature below 0^{o}C. The freezing in this process occurs at rate higher than usual and results in an increased hydraulic pressure. This phenomenon is known as super-cooling. Too much freezing after the super-cooling causes the concrete to fracture (Rosli and Harnik, 1980; Radjy et al., 1972).

2.5.1.5. Layer by layer deterioration

Concrete in presence of de-icer salt has varying salt concentration along the depth where the outer surface has lower concentration due to washout. The salt concentration gradient changes the crystallization temperature of pore water and various amount of ice forms in different layers

of concrete. The existing dilation difference between the frozen and unfrozen layers develop a considerable amount of stress which creates distress in concrete Rosli and Harnik, 1980).

2.5.1.6. Glue spall theory

Glue spall theory is the recently suggested mechanism for the concrete surface scaling which has a resemblance to the spreading of epoxy in sand blasted ornamented glass. In this mechanism, epoxy is allowed to spread on the glass at higher temperature, then the temperature of the composite is lowered which results in a thermal expansion mismatch. On the boundary of the glass, high tensile stresses are created which force the epoxy to crack into small islands leaving an exquisite tracery pattern on the glass surface. This very mechanism is applied to explain the concrete surface scaling where the ice and concrete play the similar role as epoxy and glass respectively (Gulati and Hagy, 1982; Valenza and Scherer, 2007; Sun and Scherer, 2010).

2.5.1.7. Thermal shock

Application of salt on concrete to melt the snow or ice reduces the melting point significantly depending on the salt concentration. The thermal shock is related to the application of de-icer salt and rapid concrete temperature drop. The necessary heat required to melt the ice is extracted from the concrete surface; thus, concrete suffers a super cooling due to the great heat loss. The super cooling is observed at the uppermost layer of concrete resulting in a temperature gradient which develops differential tensile stresses within the concrete (Rosli and Harnik, 1980).

2.5.2. Chemical reactions in presence of De-icer/Anti-icer salts

The existing literature suggests mostly physical damage as the contributor to the deterioration of concrete pavement but pavements can be significantly deteriorated by chemical action as well. Previous studies (Santagata and Collepardi, 2000; Lee et al., 2000; Sutter et al., 2006; Wang et al., 2006; Darwin et al., 2008; Jain et al., 2011; Shi et al., 2011; Peterson et al., 2013; Wu et al.,

2014; Farnam et al., 2015) have shown that the chemical interactions might be overshadowed by the physical effects but it can be equally significant for the deterioration of concrete pavement in the presence of de-icing and anti-icing chemicals. For instance, presence of magnesium chloride results in the decalcification of calcium silicate hydrate (C-S-H) to magnesium silicate hydrate (M-S-H) along with the leaching of calcium hydroxide (CH) due to the chemical reactions. In addition to this, the formation of Brucite (Magnesium hydroxide), Friedel's salt, Kuzel's salt and calcium oxychloride results in remarkable changes in concrete microstructure. However, the deterioration shows up in forms of map cracking, paste disintegration, loss of strength and expansion of concrete. The chemical reactions and effects involved with three commonly used de-icer and anti-icer salts are described in following subsection.

2.5.2.1. Sodium chloride (NaCl)

Various studies have shown that the presence of NaCl does not have any aggressive chemical interaction with concrete pavement unless reactive aggregates are present (Lee et al., 2000; Wang et al., 2006; Sutter et al., 2006). However, some studies have demonstrated that a pessimum NaCl salt concentration of 3%-5% by mass can cause extensive surface scaling of concrete pavement during freezing and thawing cycles (Marchand et al., 1999; Shi et al., 2010). Beyond the pessimum concentration, NaCl has exhibited a less significant amount of surface scaling (Marchand et al., 1999; Valenza and Scherer, 2006, 2007). Although, the wetting and drying events at the presence of higher concentration of NaCl solution can cause significant damage of concrete pavements (Cody et al., 1996). Furthermore, with passing time, the salt concentration in pavement concrete also builds up and thus contribute to increasing the damage. Again, NaCl containing traces of calcium sulphate and combined with the F/T action can lead to serious damage by filling the air voids with Friedel's salt and ettringite (Nicholson et al., 1999).

2.5.2.2. Calcium chloride ($CaCl_2$)

Applying calcium chloride ($CaCl_2$) on concrete pavement surface as a deicing salt, in presence of F/T cycles can cause severe damage to concrete. Calcium chloride deteriorates concrete by changing the microstructure of concrete specifically by the formation of calcium oxychloride. The calcium hydroxide, present in hydrated Portland cement, reacts with calcium chloride solution to from calcium oxychloride (Eq. i) which generates a higher magnitude of destructive crystal growth pressure. Formation of this expansive calcium oxychloride is observed, in simulated laboratory environment, just above the freezing temperature which results in a shortage of fluid ingress into concrete (Farnam et al., 2015). However, researchers have speculated that the damage caused by calcium oxychloride in the field environment is often masked by the damage caused by freezing-thawing cycles. The reaction of calcium chloride with $Ca(OH)_2$ forms calcium oxychloride according to the following reaction (Collepardi et al., 1994; Sutter et al., 2006; Peterson et al., 2013, Farnam et al., 2015).

$$3Ca(OH)_2 + CaCl_2 + 12H_2O \rightarrow 3CaO \cdot CaCl_2 \bullet 15H_2O \text{ …….. (i)}$$

Calcium chloride weakens the concrete by attacking the hydration product of C-S-H. During the reaction with hydration product, the permeability of concrete increases due to the dissolution of $Ca(OH)_2$ which increases the water availability (Sutter et al., 2006). Furthermore, concrete containing reactive dolomite aggregate experience dedolomatization reaction in presence of calcium chloride which releases magnesium to form brucite and magnesium silicate hydrate (Lee et al., 2000).

2.5.2.3. Magnesium chloride ($MgCl_2$)

Presence of magnesium chloride ($MgCl_2$) as a de-icer salt in concrete pavements is deleterious. A number of research studies have provided evidence of similar to more acute deterioration than

NaCl or $CaCl_2$ in presence of $MgCl_2$. Chemical attack on concrete induced by $MgCl_2$ results in a loss of compressive strength, volume change and development of micro-cracks (Sutter et al., 2006; Sutter et al., 2008; Shi et al., 2010). Magnesium chloride causes severe damage to concrete by producing non-cementitious magnesium silicate hydrate (M-S-H), during Mg^{2+} reaction with calcium silicate hydrate (C-S-H) (Eq. ii). Formation of M-S-H breaks down the glue that binds the aggregates together. As a consequence, the replacement of C-S-H leads to concrete crumbling and significant reduction of strength (Lee et al., 2000; Sutter et al., 2008; Shi et al., 2010).

$$C\text{–}S\text{–}H + MgCl_2 \rightarrow M\text{–}S\text{–}H + CaCl_2 \ldots\ldots\ldots\ldots \text{(ii)}$$

Formation of brucite [$Mg(OH)_2$] (Eq. iii) is also been observed in presence of $MgCl_2$ which most likely develops crystal growth pressure in concrete. Precipitation of brucite in concrete results in expansion of concrete and aggravates the associated deterioration (Cody et al., 1994; Sutter et al., 2008; Shi et al., 2010, Farnam et al., 2015).

$$Ca(OH)_2 + MgCl_2 \rightarrow Mg(OH)_2 + CaCl_2 \ldots\ldots\ldots\ldots \text{(iii)}$$

In recent studies, it has been reported that the presence of magnesium chloride forms magnesium oxychloride and secondary calcium oxychloride (Eq. iv) accompanied by severe cracking (Sutter et al., 2008; Shi et al., 2011; Peterson et al., 2013; Farnam et al., 2015).

$$3Ca(OH)_2 + CaCl_2 + 12H_2O \rightarrow 3CaO \cdot CaCl_2 \bullet 15H_2O \ldots\ldots\ldots\ldots \text{(iv)}$$

2.6. Previous Laboratory Studies

Numerous research works have been conducted, in laboratory simulated environmental conditions, to directly observe the effects of de-icer salts on concrete pavements. Different strategies have been applied to imitate the environmental conditions that concrete pavements are exposed to, including cyclic freezing-thawing, wetting-drying cycles and immersion of mortar or concrete specimens in de-icing solutions (Cody et al., 1996, Marchand et al., 1999; Lee et al., 2000; Sutter et al., 2006; Wang et al., 2006; Darwin et al., 2008; Shi et al., 2010,2011; Li et al. 2011; Jain et al., 2011; Peterson et al., 2013; Wu et al., 2014). Observations of previous works have identified that cyclic freezing-thawing action actually intensifies the physical damage despite the involvement of chemical effects in deterioration process. In wetting-drying and immersion process, the chemical effects of the de-icers investigated are developed without being masked by the physical reactions.

Physical damage due to freezing and thawing cycle can occur in the form of surface scaling and internal cracking. Surface scaling does not damage the concrete directly but it capacitates the process of higher degree of saturation; thus, leading to further deterioration. Moreover, scaling leads to the ingress of aggressive ions, making concrete susceptible to chemical reactions (Marchand and Pigeon, 1994; Valenza and Scherer, 2005; Farnam et al., 2015). It is generally believed that concrete damage by de-icer salts may initiate with the physical reaction which results in the formation of cracks and micro cracks. This increases the permeability of concrete which in turn assists the fluid and salt ion ingress inside concrete and helps to achieve the critical degree of saturation (86% saturated) leaving the concrete vulnerable to freezing and thawing damage. One of the most vulnerable zone inside concrete is the interfacial transition zone (ITZ). It is the weaker zone between coarse aggregate and cement paste which is full of voids and

vulnerable to damage. The improvement of ITZ reduces both the permeability and the likelihood of micro cracks by using lower w/c and addition of supplementary cementitious materials (i.e. fly ash). Such concrete showed better resistance to freezing and thawing damage. Addition of 6%-8% air void in the concrete improves the surface scaling and F/T resistances as well (Jain et al., 2011, 2012; Powers and Willis, 1950).

Jain et al. (2012) investigated the physical damage of F/T cycles using the actual de-icer usage concentration in the field. The samples were exposed to NaCl, $CaCl_2$ and $MgCl_2$ salt solutions where concentrations were ranging from 14 to 17% by mass. The deteriorated samples experienced massive mass loss and compressive strength loss as well. $CaCl_2$ solution was found the most harmful for the concrete samples followed by the $MgCl_2$, but no significant changes were observed in specimens exposed to NaCl solution. Similar observations and deteriorations were also reported by Wang et al. (2006) where the $CaCl_2$ solution with and without corrosion inhibitor caused significant mass and compressive strength loss. Formation of complex salt, leaching of CH and physical stresses caused by precipitation of salt within concrete pores were the major influential forces behind all the deterioration. Again, recognizing the fact that physical effect can overshadow the chemical effect, Cody et al. (1996) reported that chemical effect was the root cause of deterioration in their investigation despite the specimens were subjected to F/T exposure. In $MgCl_2$ solution, magnesium ion converted the C-S-H to non-cementitious M-S-H and formation of brucite [$Mg(OH)_2$] also worked as a major damage mechanism behind the concrete deterioration. Deterioration of $CaCl_2$ exposed concrete samples is attributed to the development of chloroaluminate and pore filling with complex salts.

The use of de-icer salt can damage the concrete cementitious materials without experiencing the freezing and thawing events. This may be attributed to the formation of Friedel's salt, Kuzel's

salt (Collepardi et al., 1994; Sutter et al., 2006) or changes occur in cement hydration product microstructure (Sutter et al., 2008; Shi et al., 2010). Several researchers have found that the principal hydration product, Calcium Hydroxide (CH), is leached out from the paste by calcium, magnesium, and chloride ions. The effect of leaching CH is significant; it leads to an increase in porosity and allows harmful chemicals to penetrate concrete easily (Carde and Francois, 1999). The detrimental effect of chloride ions on cement matrix is constant, whether the source of chloride is from sodium chloride, calcium chloride or magnesium chloride salt (Wang et al., 2006). For instance, Lee et al. (2000) exposed the specimens to F/T condition in presence of chloride salt solutions (NaCl, $CaCl_2$ and $MgCl_2$) and observed the leaching of CH to all specimens exposed to chloride ions. Furthermore, all chloride solutions resulted in paste deterioration through decalcification.

To deduct the effect of chloride ions, Santagata and Collepardi, (2000) used Calcium Magnesium Acetate (CMA) based de-icers to soak the concrete sample. It was concluded that the presence of CMA also caused the leaching of CH from cement paste. In addition, the CMA solution resulted in mass loss, reduction in load capacity, and visible deterioration. Lee et al., (2000) also observed similar incidents in case of CMA solutions and reported a severe shrinkage cracks.

A summary of effects of three commonly used de-icer salts subjected to different exposure regimes in previous studies is presented in Table 2.1.

Table 2.1: Summary of various de-icers effect in previous research investigations.

Research	Exposure	NaCl	$CaCl_2$	$MgCl_2$
Cody et al., 1996	W-D, F-T, Soak	Minor	-	-
Marchand et al., 1999	F-T	Minor	-	-
Lee et al., 2000	F-T and W-D	Minor	Significant	Significant
Sutter et al., 2006	Soak	Minor	Significant	Significant
Wang et al., 2006	F-T and W-D	Minor	Significant	Significant
Darwin et al., 2008	W-D	Minor	Significant	Significant
Shi et al., 2010	F-T	Significant	-	Minor
Shi et al., 2011	Soak	Minor	Significant	Significant
Jain et al., 2012	W-D, F-T, Soak	Minor	Significant	Significant
Peterson et al., 2013	Immersion	Minor	Significant	Significant

2.7. Previous Field Studies

Concrete pavements in cold climate regions are expected to provide a fairly long-term service life. However, in recent times, premature joint deterioration has been detected in concrete pavements in these regions where areas adjacent to the longitudinal and transverse joints are mostly reported to be affected. Previous in-situ investigations (Rangaraju, 2002; Olek et al., 2007; Yang et al., 2011; Taylor et al., 2011; Kang et al., 2012;Arribas-Colón et al., 2012;Jones et al., 2013 and Panchmatia et al., 2014) aimed at finding the root causes of premature joint

deterioration concluded that structural design (i.e. joint spacing, saw cut depth), construction practices (i.e. water-cement ratio, vibration rate) and material properties (i.e. air void quality) can be linked to the premature joint deterioration of concrete pavements. Various reactions and mechanisms are also responsible for the deterioration of concrete pavement such as F/T cycles, degree of saturation, alkali aggregate reaction and sulfate attack. In each of these deterioration mechanisms, water carrying aggressive ions such as chloride or sulfate, is involved in the degradation process. The intensive use of de-icing salts is considered to be a primary cause of the deterioration of concrete pavement in cold climates. De-icing salts can penetrate into the concrete and change the concrete microstructure by participating in aggressive chemical reactions (Sutter et al., 2006; Wang et al., 2006; Darwin et al., 2008; Jain et al., 2011; Peterson et al., 2013; Panchmatia et al., 2014).

The signs of premature deterioration are not initially visible; however, they are observed after a considerable amount of damage had taken place in the joint areas. The damage may initiate at the bottom and advance towards the top surface resulting in joint spalling, huge mass loss and cracking at and near the joint areas. Previous in-situ evaluation (Jones et al., 2013) of the affected pavement areas (joints) revealed that in many cases, the joints continued to hold water (solution) long after the wetting event (Figure 2.7). Micro-cracks, close to the joints, are saturated with trapped water, thus shadowing may often appear. Where shadowing is observed, the system is not well drained and subsequently the joint exhibits significant loss of material. Furthermore, it has been observed that where the joints were damaged, generally the sealant had failed and a ‘Bulb’ shaped damaged zones were spotted underneath the sealed joints in some cases (Arribas-Colón et al., 2012).

Figure 2.7: Joint deterioration of concrete pavement

Rangaraju (2002) and Olek et al. (2007) suspected F/T effect as the main culprit behind the premature joint deterioration. The quality of air void distribution (characterized by spacing factor), their average size and volume (characterized by specific surface area) are significant to the F/T resistance of concrete pavements. Addition of excessive water during mixing and excessive paver and supplemental vibration around joint areas during construction may contribute to insufficiency of air voids in the system leaving the concrete vulnerable to F/T damage (Rangaraju, 2002; Panchmatia et al., 2014). Presence of secondary deposits infilling air voids has been observed in deteriorated concretes. Petrographic analysis of deteriorated pavement joint cores (Rangaraju, 2002; Olek et al., 2007; Arrobas-Colón et al., 2012; Panchmatia et al., 2014) revealed the presence of ettringite and Friedel's salt in filled air voids which compromises the air quality required to sustain in colder environment (Figure 2.8). The secondary deposits are assumed as precipitates caused by repetitive saturation of air voids with mineral laden water. The elongated existence of moisture in joints results in an increased saturation level; which, causes the concrete to reach critical saturation level leaving concrete vulnerable to F/T damage and cracks (Olek et al., 2007). Some researchers (Olek et al., 2007, Taylor, 2011, Olek, 2013; Panchmatia et al., 2014) speculated that the infilled air voids would

serve as a centre of pressure for the progression of secondary deposit precipitation, resulting in crack formations.

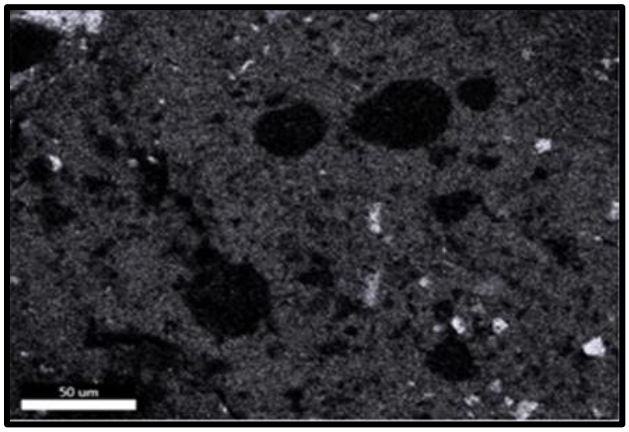

Figure 2.8: Infilling of air voids with secondary deposits.

Though the root causes behind the premature joint deterioration may differ considering the pavement concrete construction, drainage facility, exposure to de-icer salts etc. but recent studies on laboratory concrete (Sutter et al., 2006, Jain et al., 2011, Peterson et al., 2013) indicate that chloride-based salts (magnesium chloride, calcium chloride, sodium chloride) may have accelerated the pavement F/T deterioration. Therefore, the air voids of deteriorated concrete might have filled with secondary deposits such as ettringite and Friedel's salt.

2.8. Closure

Extensive research has been done on concrete pavement deterioration in presence of de-icer salts under freezing-thawing exposure conditions. Yet, limited research work has been conducted considering the salt concentration based on phase diagram where solution and ice co-exist in the system and relevant with the in-service situation. On the other hand, most of the previous research investigating de-icer salt effect on concrete pavement considered the salt solutions consisting of equal mass of de-icing salt or an equal molar concentration (equal amount of substance in a given volume). However, according to phase diagram, the ice melting capacity of

de-icer salts is more closely related to the concentration of chloride ions present in a given quantity of water rather than the mass or molar concentration of the de-icer. Therefore, further research is required to investigate the freezing-thawing damage of concrete pavement in presence of de-icer salts considering the equal chloride ion concentration and existence of ice with salt solution.

Furthermore, most laboratory simulation work on freezing-thawing exposure has been performed using conventional pavement concrete mixtures. Research is still required to investigate the effect of key parameters such as the type and amount of supplementary cementitious materials (SCMs) and the response of pore structure characteristics on the concrete vulnerability to this kind of distresses. In addition, the concrete industry is under the auspicious influence of nanoparticles impact to improve the long-term performance of concrete infrastructures. As the research on nano-modified concrete is still focused on hydration kinetics and physio-mechanical properties, there is a lack of research data on the nano-modified concrete durability characteristics, especially its resistance against de-icer salts. To date, no research investigation has focused on the performance of nanoparticles such as nanosilica combined with SCMs and cement-based materials to de-icing salts under the F/T exposure condition. Again, the introduction of Portland Limestone Cement (PLC) in North America is relatively new and the dearth of long-term performance data in these conditions requires further focused research investigation.

Considering the abovementioned facts, this research work aims at investigating the performance of novel concrete mixture designs, incorporating General use and Portland limestone cement, Class F fly ash and nano particles (e.g. nanosilica), against the F/T damage resistance in presence of de-icer salts.

3. Experimental Program

This chapter illustrates in details the materials, mixture design, exposures and experimental methods adopted for the two phases (experimental analysis on field cores and laboratory specimens) carried out in this research program.

3.1. Field Work

To evaluate the concrete pavement that has been directly (regional roads) and indirectly (residential streets) exposed to de-icing salts during winter, concrete cores from different regional roads and residential streets in the city of Winnipeg, Manitoba were collected. Concrete cores from both deteriorated and sound pavement sections at or near the longitudinal and transverse joints from various streets were extracted. The general description and graphical representation of the locations from where the cores were obtained are illustrated in Table 3.1 and Fig. 3.1.

Table 3.1**:** Description of extracted core location

Code	Specific Area
A	Damaged transverse joint
B	Damaged longitudinal joint near the transverse joint
C	Damaged longitudinal joint away from the transverse joint
D	Damaged area from wheel path away from transverse joint
E	Undamaged transverse joint
F	Undamaged longitudinal joint

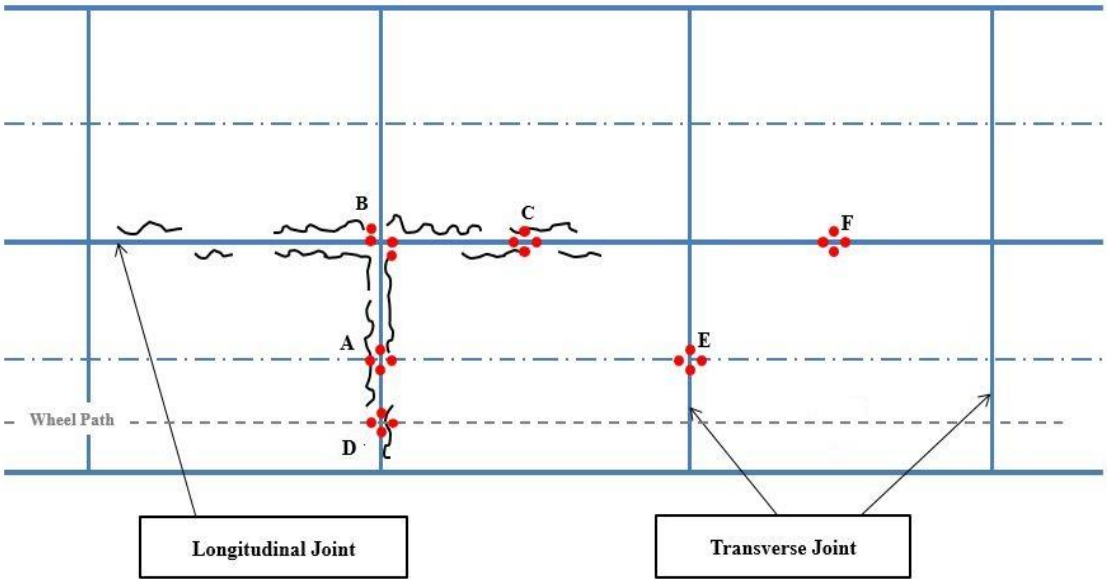

Figure 3.1**:** Acquired concrete core locations

3.1.1. Description of field sites and data collection

Representative pavement sections (regional roads and residential streets) were chosen by Public Works Department, City of Winnipeg (COW) at an urban zone in the central area of Winnipeg, Manitoba. The pavement in the test location is subjected to large temperature changes, as the maximum and minimum air temperatures during the last 10 years were +36°C and –36°C, respectively. The investigation started with a detailed inventory of the pavement sections chosen in order to identify and classify the existing types of distresses and select candidate locations for extraction of the cores. The available information of the history of these pavement sections was documented, as listed in Table 3.2, to informatively provide important preliminary information regarding the potential causes of deterioration. Generally, concrete with target performance of 35 MPa and meeting a class of exposure C-2 (plain concrete subjected to chlorides and freezing-thawing) according to CSA A23.1 (CSA 2014) was used in all roads under investigation.

Typically, the concrete comprised General Use (GU) portland cement and up to 15% fly ash (Class F), as a supplementary cementitious material (SCM), meeting the requirements of CSA A3001 (CSA 2013), and the water-to-cementitious materials ratio (w/cm) was in the range of 0.36 to 0.38.

According to COW policy for ice control (Policy on Snow Clearing and Ice Control 2011), the regional roads have been classified as priority I streets where de-icers (mainly chloride-based salts: salt brine with a concentration of 23.3% of sodium chloride by weight) are directly used in winter months to provide an adequate level of service by preventing the formation of ice on the roadway surface due to freezing rain, fog, and traces of snow (anti-icing). Moreover, a liquid salt (proprietary solution comprising 26.6% calcium chloride, 3.1% magnesium chloride, 1.3% sodium chloride and 0.9% potassium chloride) are also added to abrasives (sand) or solid salts to make them easier to manage and distribute, and help them stay on roads (pre-wetting). The pre-wetting chemical is applied at 40 l/ton for treated sand and 50 l/ton for road salt. The rates of application for these de-icers are shown in Table 3.2 In contrast, the existing policy for ice control states that the residential streets (priority II) are maintained to a compacted snow/ice by plowing operations without applying salts, except for specific areas as described in Table 3.2.

Table 3.2: Available information on the history of the pavement sections

	Residential street I	Residential street II	Regional road I	Regional road II
Year paved	2001	1999	1996	1996
No. of lanes	2 (traffic lane/ parking lane)	2 (traffic lane/ parking lane)	3 (3 traffic lane/ parking lane)	3 (2 traffic lane/ shoulder)
Average traffic/day (vehicles)	< 2500	< 2500	> 20000	> 20000
Design speed (km/h)	40 - 50	40 - 50	60 - 80	60 - 80
Salt application (kg/lane kilometer) [Avg. frequency/winter]	Not recommended	Not recommended	160 [14]	160 [18]
Treated sand* **(kg/lane kilometer)**	Specific areas**	Specific areas**	320	320

*Liquid salt is added to the sand (5% by weight).
**Intersections, pedestrian corridors and crosswalks, railway crossings and inclinations.

3.2. Laboratory Simulation

A wide range of novel concrete mix designs incorporating General use (GU) portland cement and Portland limestone cement (PLC, comprising 6% to 15% inter-ground limestone powder with clinker), Class F fly ash and nanoparticles (nanosilica), were designed to achieve the objectives of this research program. To evaluate the performance of newly developed binary and ternary mixtures in extreme cold condition and make a comparison with the regular concrete mixture (used generally in North America), all the concrete specimens were subjected to freezing-thawing (F/T) exposure condition in simulated laboratory condition in an environmental chamber.

3.2.1. Materials and mixtures

For the preparation of concrete mixtures, general use (GU) Portland cement, Portland limestone cement (PLC) and Type F fly ash (FA), which meet the requirements of CAN/CSA- A3001 (CSA3001, 2013; cementitious materials for the use in concrete) standard were used as the main components of the binders. Table 3.3 illustrates the chemical composition and properties of the cement and supplementary cementitious material (SCMs) [fly ash] used in this work. In addition, to modify the concrete properties ultrafine nanoparticles (nanosilica) [aqueous solution with 50% solid content] were incorporated in some mixture designs. The physical properties of this nanoparticle is enlisted in Table 3.3 as well. Locally available coarse aggregates (natural gravel with maximum size of 9.5 mm) and fine aggregates (well-graded river sand with fineness modulus of 2.9) were used. The specific gravity and absorption for gravel was 2.65 and 2%, respectively, while the sand had 2.53 and 1.5% specific gravity and absorption, respectively. To ensure the desirable workability for mixed concrete, a high range water reducing admixture (HRWRA) based on polycarboxylic acid and complying with ASTM C494-C494M (ASTM C494, 2012; Standard Specification for Chemical Admixtures for Concrete) was added to all the mixtures in the range of 0 to 2000 ml/100 kg binder to maintain a slump range of 75 mm. to 120 mm. An air void content of 6 - 8% was achieved by adding an air-entraining admixture according to ASTM C233/C233M (ASTM C233, 2014; Standard test method for air-entraining admixtures for concrete) in all concrete mixtures.

Table 0.3**:** Physical and chemical properties of used cement and SCMs.

	GU	**PLC**	**Fly Ash**	**Nanosilica**
Chemical Composition				
SiO_2 (%)	19.8	19.2	56.0	99.2
Al_2O_3 (%)	5	4.4	23.1	0.38
Fe_2O_3 (%)	2.4	2.6	3.6	0.02
CaO(%)	63.2	61.5	10.8	--
MgO(%)	3.3	2.4	1.1	0.21
SO_3 (%)	3.0	3.4	0.2	--
Na_2O (%)	0.1	0.2	3.2	0.2
Physical Properties				
Fineness (m^2/kg)	390	460	290	80,000
Specific Gravity	3.17	3.08	2.12	1.4

A total of 12 concrete mixtures were prepared in this study. The total binder content in all the mixtures was kept constant at 400 kg/m^3 and the water-to-cement ratio was also kept constant at 0.40, representing the typical values for pavement concrete mixtures in North America. The mixture design variables were types of binder (GU or PLC cement, GU blended with fly ash or PLC blended with fly ash), and inclusion of nanoparticle (nanosilica). The mixture IDs were coded according to the type of cement, amount of fly ash and type of nanoparticle used. For instance, GUF20 was prepared with GU cement and 20% fly ash and PLCF30S was prepared with PLC cement, 30% fly ash and 6% nanosilca. The proportions of materials used to prepare all the concrete mixtures are presented in Table 3.4.

Table 0.4**:** Proportions of mixtures per cubic meter of concrete

Mixture ID.	Description	Cement (kg)	Fly Ash (FA), (kg)	Nano silica (NS),(kg)	Water (kg)	Coarse Agg., (kg)	Fine Agg., (kg)
GU	GU, single	400	--	--	160	1,096	590
GUF20	GU, binary, FA	320	80	--	160	1,077	580
GUF30	GU, binary, FA	280	120	--	160	1,068	575
GUS	GU, binary, NS	376	--	48	136	1,091	587
GUF20S	GU, ternary, FA, NS	296	80	48	136	1,072	577
GUF30S	GU, ternary, FA, NS	256	120	48	136	1,063	573
PLC	PLC, single	400	--	--	160	1,096	590
PLCF20	PLC, binary, FA	320	80	--	160	1,077	580
PLCF30	PLC, binary, FA	280	120	--	160	1,068	575
PLCS	PLC, binary, NS	376	--	48	136	1,091	587
PLCF20S	PLC,ternary, FA, NS	296	80	48	136	1,072	577
PLCF30S	PLC,ternary, FA, NS	256	120	48	136	1,063	573

3.2.2. Procedures

All the materials were mixed in a high-shear mixer according to ASTM C192 (ASTM C192, 2014; Standard Practice for Making and Curing Concrete Test Specimens in the Laboratory). A specific sequence of mixing was implemented based on experimental trials to achieve homogenous dispersion of constituent materials. At the beginning, the aggregates were mixed for 30 seconds after approximately 15% of the mixing water was added. Subsequently, the cement and SCMs were added to the aggregate and mixed together for 1 minute. The admixtures (air-entraining admixture and HRWRA) and the colloidal nanosilica, if any, were added to the remaining water while stirring vigorously for 45 seconds to obtain a liquid phase containing well-dispersed nanoparticles and admixtures. Finally, the liquid phase was added to the binder and aggregates and the mixing continued for 2 more minutes. A vibrating table was used while casting to ensure good compaction of the specimens. Polyethylene sheets were used to cover the surfaces of specimens for 24 hours. Then, the specimens were demolded and cured in a standard curing room (maintained at a temperature of 22±2^{o}C and relative humidity of more than 95%) according to ASTM C192 (ASTM C192, 2014) for 28 days.

3.3. Exposure

The concrete specimens were subjected to cyclic F/T exposure according to the general procedure of ASTM C666 test procedure-A with few exceptions. De-icing solutions were used instead of water and a low frequency of F/T cycle per day was used to eliminate the effect of physical action masking the chemical reactions. Lastly, the F/T cycles were continued up to 600 cycles instead of 300 cycles. All the samples were kept in plastic container immersed in respective de-icing salt solution and placed in an environmental chamber, as shown in Fig. 3.2, for F/T exposure. The concrete samples were immersed in respective salt solutions for 3 days

before exposing to the F/T condition. The duration of one F/T cycles was 12 hours: freezing at −18±1°C for 7 h and thawing at 4±1°C for 3.5 h, and 45 min. to ramp to the minimum freezing temperature or the maximum thawing temperature. Every two weeks, the samples were brought outside of the environmental chamber for visual observation and to measure the mass and length change along with the change in relative dynamic modulus of elasticity (RE_d) of the concrete specimens. When any specimen showed considerable surface damage or reduction in RE_d value of more than 80% of the initial value, then the exposure regime was terminated for the specimen and samples were reserved for microstructural analysis.

Figure 3.2: Environmental chamber used for F/T exposure.

3.3.1. De-icing salts

The effect of de-icing salts on concrete pavement was evaluated by using three types of de-icing salts (NaCl, $MgCl_2$ and $CaCl_2$). The ion chromatography method (chloride ions analyzed using

ion chromatographs with the typical detection method for electric conductivity of ions) was used to maintain the same ionic concentration of chloride ions in each type of salts and to eliminate the drawbacks of using salt concentration of either equal mass of de-icing salts or equal molar concentration. The concentrations of the de-icing salts are listed in Table 3.5. The eutectic point refers to the theoretical melting point of the de-icing salt which also distinguishes the liquid phase from the solid phase in a salt solution. Moreover, the eutectic point corresponds to the lowest temperature at which that particular salt can melt ice/snow. The rationale for the selected concentration of salt in this research work is to achieve both the solid and liquid phase at the same time when the solution is under freezing condition. The salt solutions were renewed every four weeks to maintain a continual supply of de-icing salts similar to in-service conditions. Hence, the physical and chemical effects of F/T in presence of de-icing salts on newly developed concrete mixtures were evaluated.

Table 3.5: Concentration of selected de-icing salts

Type of Salt	Salt Concentration by Mass (%)	Chloride Concentration (mols/l)	Chloride Concentration (ppm)
Sodium Chloride (NaCl)	14.2	2.83	100,530.28
Magnesium Chloride ($MgCl_2$)	11.9	2.83	100,737.80
Calcium chloride ($CaCl_2$)	13.6	2.83	100,737.80

3.4. Tests

3.4.1. Bulk tests on extracted pavement cores

The interconnectivity of extracted concrete pavement cores was assessed by Rapid Chloride Penetrability Test (RCPT) according to ASTM C1202 specification (ASTM C1202, 2012; Standard Test Method for Electrical Indication of Concrete's Ability to Resist Chloride Ion Penetration). Concrete discs with 50 mm thickness were cut from the field cores to conduct the RCPT. The side surfaces of all the concrete discs were coated with rapid setting epoxy and subsequently the concrete discs were placed inside a desiccator under vacuum pressure for three hours without water and one hour with de-aerated water. After 18 hours of soaking in water, the concrete discs were mounted between cathodic (3% NaCl solution) and anodic (0.3 % NaOH solution) compartments under a potential difference of 60 V DC for 6 hours. The data acquisition system connected to the cells automatically collected charges passing through the discs (in coulombs) during the test period. The test setup for the RCPT is illustrated in Fig. 3.3. To avoid the electrolysis bias of this method, the penetration depth of chloride ions into concrete, which better correlates to the physical characteristics of the pore structure, was determined according to Bassuoni et al.(2006). To measure the physical penetration depth of chloride ions, after finishing the RCPT, the discs were axially split and sprayed with 0.1 M silver nitrate solution, which forms a white precipitate of silver chloride in approximately 15 minutes. The depth of the white precipitate was determined at five different locations along the diameter of each half specimen. The average depth is considered to be an indication of the ease of ingress of chloride ions, and thus the connectivity of the microstructure (Bassuoni et al., 2006).

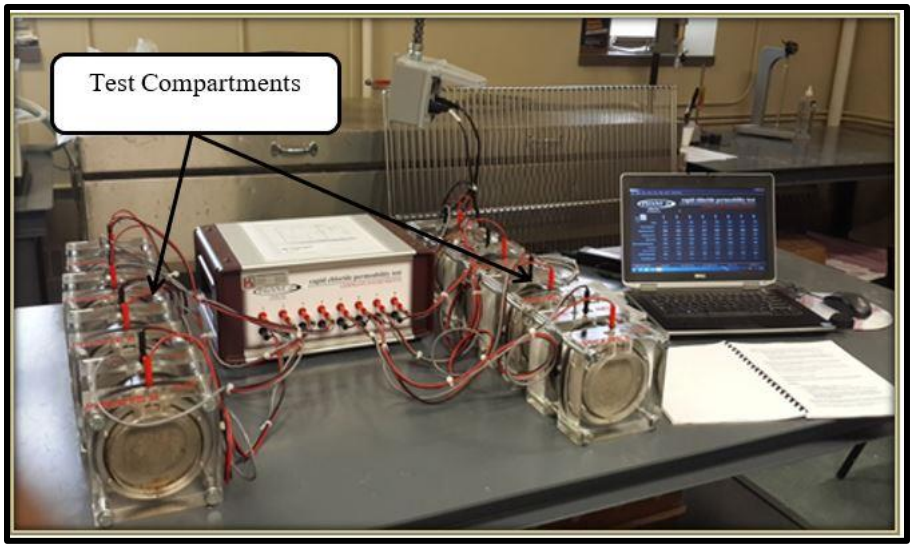

Figure 3.3: Test set up for RCPT

The transport properties of the concrete cores were assessed by capillary absorption test. The absorption test was conducted on previously conditioned (dried at a temperature of 50±2 °C and a relative humidity (RH) of 40% for 72 h followed by vacuum pressure (~85 KPa) for 6 h) concrete discs of irregular sizes and shapes which were cut from the collected cores according to Tiznobaik and Bassuoni (2017). The initial mass to the nearest 0.01 g was recorded and then the specimens were submerged in 4% calcium chloride solution for up to 360 min, and the amount of absorption after 1, 5, 10, 20, 40, 80, 160 and 360 min were recorded and normalized by the initial mass (dry mass) of the specimens. To complement the results of the absorption and RCPT tests, the characteristics of the pore structure of concrete were determined by mercury intrusion porosimetry (MIP) (Fig. 3.4) with a maximum pressure of 206 MPa, allowing the detection of pore radii ranging from 3 nm up to 1000 µm. Small pea-sized chunks (around 5-10 mm in size) taken from at least two replicate cores were carefully selected to avoid the inclusion of large aggregates. The chunks were oven-dried at 45±5 °C for 72 h; then, they were kept in a desiccator containing calcium sulfate for 24 h before the MIP test. This method of drying at a lower temperature for a longer period was adopted to avoid the formation of micro-cracks, which may

occur at higher drying temperatures. The contact angle and the surface tension of mercury were taken as 130º and 485 dynes/cm, respectively.

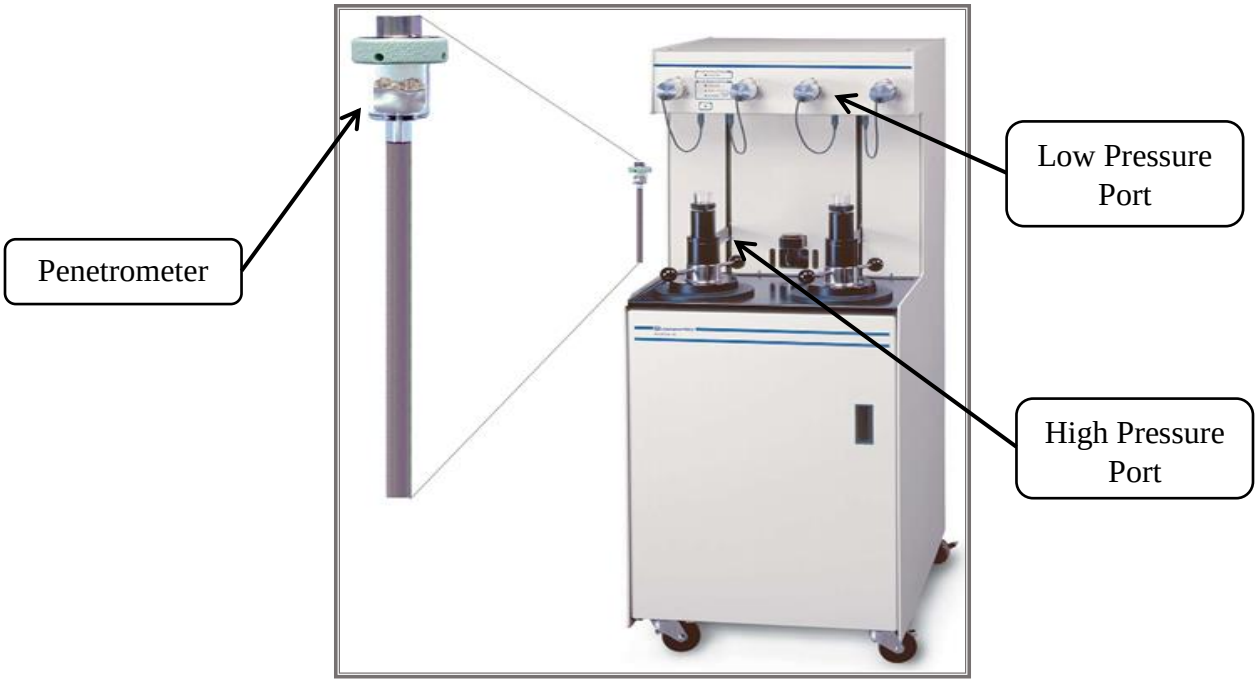

Figure 3.4: MIP apparatus.

To characterize the air-void system in the concrete cores, the automated flatbed scanner method described by Chatterji and Gudmundsson (1977) was used on a square cross section of 100 mm cut pieces from the cores. This method is based on painting the surface of concrete in black, and then forcing white powder of wollastonite into the air-voids so that the voids are visible in scanning and image analysis. This method provides repeatability and a good level of accuracy as reported by previous studies (Zalocha and Kasperkiewicz 2005).

3.4.2. Microstructural, mineralogical and thermal analyses of pavement cores

For the identification of underlying damage mechanism and the alteration in microstructure, the deteriorated concrete specimens were studied by microscopy, thermal and mineralogical analyses. To detect the mechanism of failure and difference in reaction products, fracture concrete surfaces were extracted from the surface (up to 20 mm depth) of the pavement cores to

be examined by scanning electron microscopy (SEM) assisted with energy-dispersive X-ray analysis (EDX). A visual representation of the used SEM sample chamber is shown in Fig. 3.5. The samples were coated with a fine layer of carbon before performing the analysis to make the surface conductive and to improve the sample imaging. To complement the analysis of the SEM, the reaction products within the cementitious matrix, were analyzed by X-ray diffraction (XRD, Cu-Kα) on powder samples collected from the surface (0-20 mm from the exposed surface) of selected specimens. The XRD device is presented in Fig. 3.6. This powder was prepared from carefully extracted fracture pieces (not including large coarse aggregate) of specimens, which were pulverized to fine powder passing through sieve #200 (75 µm). Samples were collected from the deteriorated concrete specimens and pulverized to fine powder to detect the formation of sulfate-bearing products in cementitious matrix. For XRD, scan speed of 2°/min and sampling interval of 0.01° 2θ was used for all the samples. Furthermore, the samples were heated up to 500°C with a ramp temperature of 5°C/min in the DSC tests (Fig. 3.7).

Figure 3.5: SEM sample chamber where the fracture pieces were mounted

Figure 3.6: XRD instrument where the powder samples were mounted

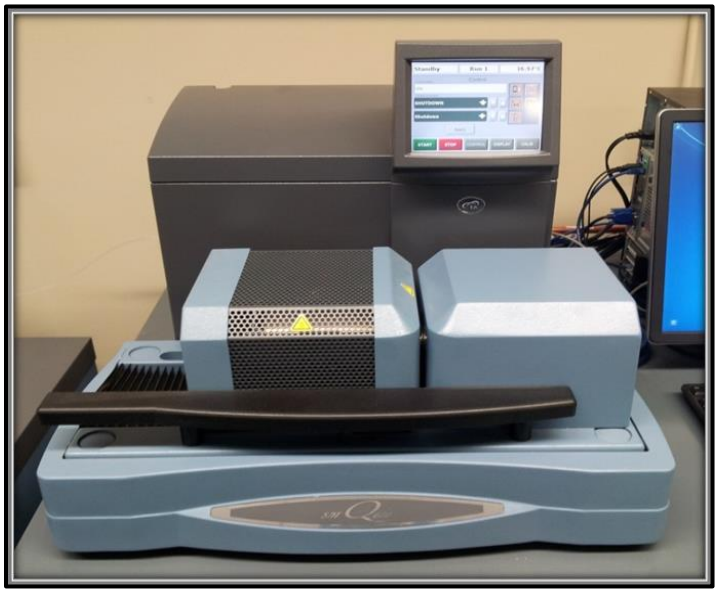

Figure 3.7: DSC instrument where the powder samples were mounted.

3.4.3. Tests on laboratory freezing-thawing exposure specimens

To comprehend the effects of de-icing salts in F/T exposure on the expansion of specimens, this study considered the comparative length change of the concrete prisms due to possibility of

expansion. Fig. 3.8 shows the comparative length change apparatus. In case of mass change, the initial mass value was used to calculate the mass change versus time of exposure for concrete specimens exposed to different de-icing salt solutions. The internal damage (development of micro-cracks) of concrete prisms exposed to continued freezing and thawing conditions, was evaluated by the comparison of dynamic modulus of elasticity. According to ASTM C215 (Year; Standard Test Method for Fundamental Transverse, Longitudinal, and Torsional Resonant Frequencies of Concrete Specimens) the dynamic modulus of elasticity of all the specimens was recorded and RE_d (change in dynamic modulus of elasticity over time) was determined. The test setup for the dynamic modulus of elasticity measurement is shown in Fig. 3.9. To detect the mechanism of failure and difference in reaction products, concrete specimens were studied by microscopy, thermal and mineralogical analyses. The SEM and XRD were conducted according to the procedure described in section 3.4.2.

Figure 3.8: Length comparator utilized for determining the change in length of concrete prisms.

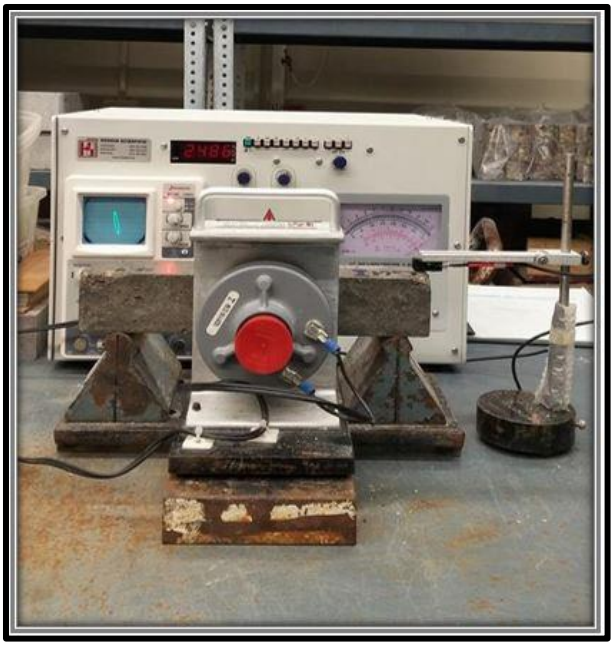

Figure 3.9: Sonometer apparatus used to determine the dynamic modulus of elasticity

4. Results and Discussion of the Field Study

4.1. Visual observations

A condition assessment survey was filled out for each site visited, incorporating information about the general description of the surrounding environment, drainage system, maintenance, sealant condition, visual damage. The extent of damage on the surface and along joints was observed and described as minimum, medium (considerable), or high (extensive) for each site. The visual inspection provided reasonable information about possible factors affecting the damage.

For regional roads, most of the sites showed distinctive signs of damage (Fig. 4.1). The visual evaluation of the condition of these sites revealed that the drainage of the joints contributed significantly to their performance. The drainage system suffered from differential movement of slabs (i.e. change of slope) in many locations, debris, natural siltation, vegetation, and lack of proper maintenance. Most joints continued to entrap water (solution) long after wetting events (Fig. 4.1a), which also can be linked to insufficient permeability within the base and sub-base layers. Thus, notable darkening (shadowing) of the concrete near the transverse and longitudinal joint was visible (Fig. 4.1b). The darkening indicated the accumulation of dirt and other road debris and high moisture content within the micro-cracks along and near the joints. Joint sealants were mostly de-bonded from both sides of the saw-cut joints (Fig. 4.1c). The most intensive damage occurred at the intersection of the transverse and longitudinal joints, where these areas exhibited significant loss of material. Therefore, based on the visual evaluation of the condition of these sites, the extent of damage was considered as ‘medium or high’ deterioration in both

longitudinal and transverse joints. Due to the differences in the pavement conditions for the streets selected, the cores had been extracted from different sections at and adjacent to the joints.

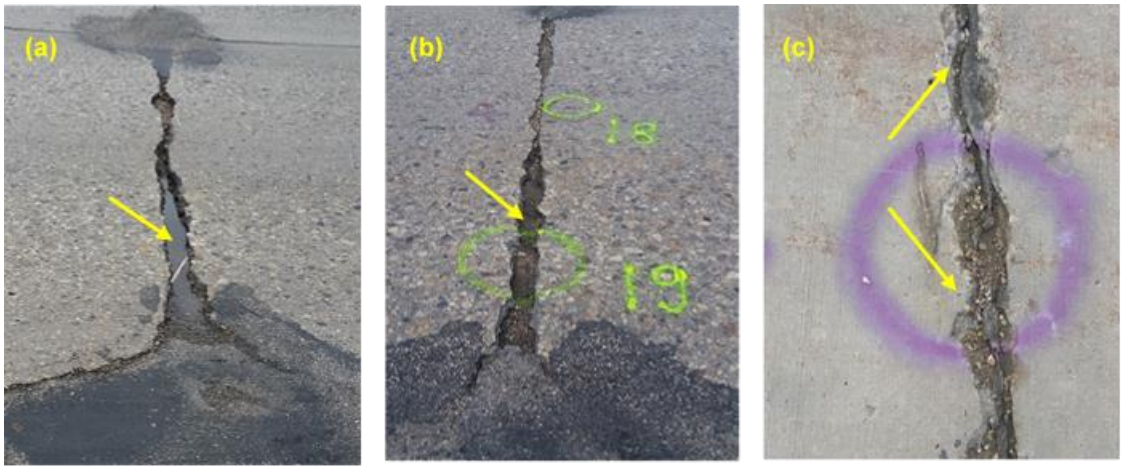

Figure 4.1: Evidence of joint deterioration in regional roads: (a) widening of joints and entrapment of water/solution, (b) accumulation of dirt and other road debris, and (c) de-bonded sealants.

In many cases, the damage to the joints was extensive and the concrete crumbled during the coring process (Fig. 4.2a); therefore, it was not possible to obtain full cores in these locations, where they ended up into several pieces, as for example shown in Fig. 4.2b. Parallel cracks were also a common damage feature of concrete cores in these locations (e.g. Fig. 4.2c), and the damage was generally found in both top and bottom parts (Fig. 4.2d).

Figure 4.2: An example from regional roads showing: (a) damage of concrete during the coring process, (b) fractured cores, (c) sub-parallel cracks in the extracted cores, and (d) damage of top and bottom parts.

In comparison to the regional roads, the residential streets were in excellent conditions, except that the concrete surface occasionally exhibited surface scaling and pop-outs in the parking lane. Most of the joints were clean and sound, and there was no evidence of faulting or spalling (e.g. Figs. 4.3a). The pavement cross slop and drainage system appeared to be effective as water continued draining after wet events as adequately as designed. During coring, it was observed that core holes drained well compared with core holes of regional roads. Also, the cores extracted at and near joints appeared sound and intact; they were cleanly and fully drilled with excellent conditions (e.g. Fig. 4.3b).

Figure 4.3: An example from a residential street showing: (a) sound joint without evidence of faulting or spalling, and (b) whole/intact core.

4.2. Transport properties

Most durability issues of concrete pavements, particularly under aggressive environments such as F/T and W/D cycles, are controlled by the pore structure characteristics and transport properties of concrete. The porosity of concrete and interconnectivity of the pore structure are key parameters for understanding the transport of fluids and ionic species into concrete, which indicates the ease of saturation of concrete, and in turn its vulnerability to damage. Therefore, a series of tests were carried out to identify the pore structure characteristics for the cores extracted from different locations in both regional and residential streets. All the results of absorption, RCPT, and MIP tests were statistically evaluated by the Analysis of Variance (ANOVA) method at a significance level (α) of 0.05. According to ANOVA, exceeding the critical value (F_{cr}) of an *F*-distribution density function reflects that the tested variable significantly affects the mean of the results (Montgomery 2014).

Water absorption test indicates mass transport of fluids into concrete by capillary suction (Hall 1989). The rate and total absorption were determined for at least six samples from each location in both regional and residential streets, as shown in Fig. 4.4. It can be noted that the general trend

of the absorption curves indicates significant (Table 4.1) difference between the cores extracted from the regional and residential streets. For example, the initial absorption, at 1 min, for the cores extracted from the residential and regional streets gained about 25% and 55%, respectively of their total absorption after 360 min. Also, the rate and total absorption values for the cores extracted from the regional streets are significantly higher (two to three times) than that of the cores extracted from the residential streets.

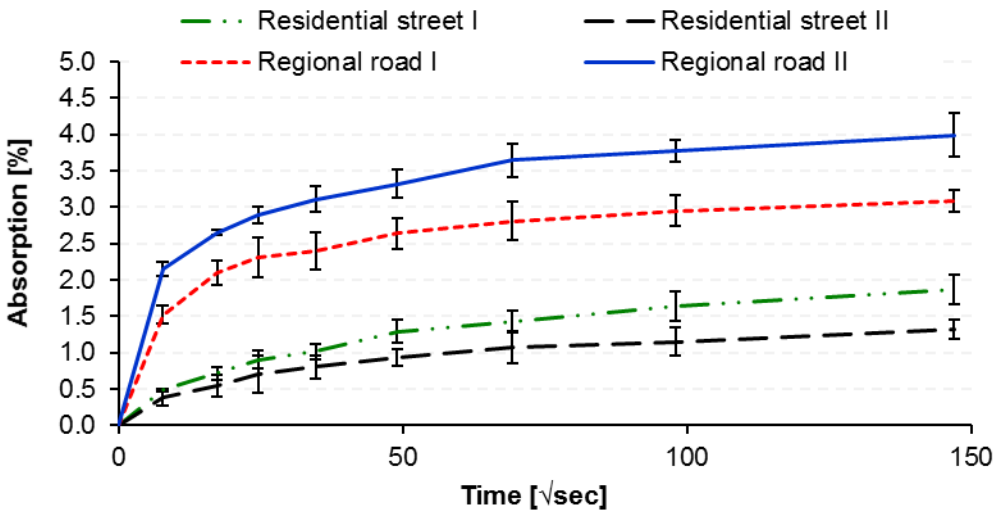

Figure 4.4: Rate of water absorption of cores extracted from different pavement sections.

Table 4.1: ANOVA for the total absorption, migration coefficient and total porosity results of the cores extracted from different streets

Test	***F***	***P-Value***	F_{cr}	**Effect**
Absorption test Absorption %	90.45	0.001	4.20	Significant
RCPT Migration coefficient	189.12	9.95E-14	4.49	Significant
MIP Total Porosity %	29.68	0.003	18.51	Significant

The trends of the absorption test conformed to the measured penetrability (Table 4.2) of concrete in these locations. The cores obtained from regional streets were classified as “Moderate to High” penetrability according to ASTM C1202 (ASTM 2012), indicating coarse and continuous

pore structure. Comparatively, specimens from residential streets generally had "Very Low" penetrability. The classification of chloride ions penetrability was consistent with the chloride diffusion coefficients (non-steady-state migration coefficient) of these cores. The chloride migration coefficient of concrete was calculated on the basis of the penetration depth (Table 4.2 and Fig. 4.5) according to NT BUILD 492 (1999), to account for the effect of heat (Joule) and different testing durations on ionic mobility within specimens. These factors particularly affected samples with high porosity and considerable contamination with chloride ions. Among all the cores tested, cores from regional road II had the highest migration coefficient (average of 54.46 $\times 10^{-12}$ m^2/s), conforming to the earlier observations of the absorption test. Despite a "Moderate" penetrability in some cores extracted from regional roads, their penetration depth was very high (50 mm). The values of passing charges observed in these samples may be attributed to the Joule effect as these samples reached the maximum temperature (70°C) allowed by the apparatus before the end of testing; subsequently, the test stopped before collecting the actual passing charges after 6 hours. It seems that applying de-icing salts altered the transport properties of the concrete in the regional roads. It was reported that de-icing salts may cause leaching of calcium hydroxide from the hardened cement paste, resulting in higher porosity of concrete (Wang et al. 2006), as discussed later in the TG and microscopy section.

Table 4.2: Rapid chloride penetrability test (RCPT) results

	Passing charges (coulombs)	**Chloride ion penetrability class (ASTM C1202)**	**Average penetration depth (mm) [standard error]**	**Migration coefficient ($\times 10^{-12} m^2/s$)**
Residential street I	327	Very Low	9 [0.74]	1.62
	1013	Low	15 [1.29]	5.55
	456	Very Low	10 [0.69]	2.24
	846	Very Low	12 [1.01]	3.51
Residential street II	112	Very Low	11 [0.49]	2.87
	216	Very Low	13 [0.79]	4.10
	103	Very Low	10 [1.09]	2.22
	401	Very Low	8 [0.69]	1.72
Regional road I	2864	Moderate	50 [0]	31.37
	4832	High	50 [0]	34.02
	3120	Moderate	43 [0.64]	27.30
	5143	High	50 [0]	35.39
Regional road II	4689	High	50 [0]	81.47
	4989	High	50 [0]	49.47
	5223	High	50 [0]	53.26
	4930	High	50 [0]	33.62

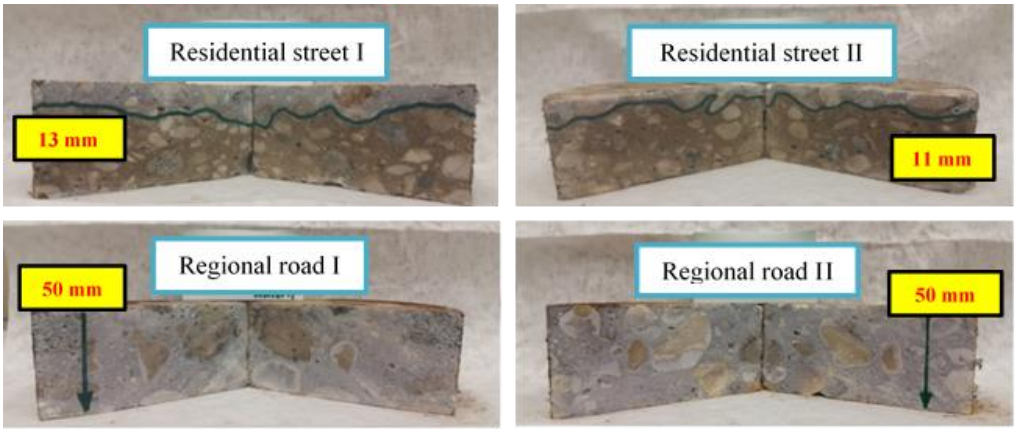

Figure 4.5: Whitish color showing the chloride penetration.

The MIP results (cumulative intrusions, porosity, threshold pore diameters and proportion of micro-pores [less than 0.1 µm]) for all the field cores are listed in Table 4.3. The MIP tests were done on at least four small chunks extracted from two replicate cores for each street, which were put in the same test compartment (porosimeter). Thus, the results shown in Table 4.3 can be reasonably considered the averages of representative populations to the physical features of microstructure for the concrete cores tested in this study. The trends of MIP conformed to the transport properties (absorption and penetrability/diffusivity) determined for these cores in the sense that there was a significant (Table 4.1) increase in the proportion of macro-pores, threshold pore diameter, and total porosity of the cores extracted from regional roads relative to the cores extracted from residential streets (Table 4.3). For example, the total porosity for the concrete extracted from regional roads was 58% higher than that of corresponding cores extracted from the residential streets. Also, the threshold pore diameter for these cores was, approximately, 3 µm, which was one order of magnitude higher than the lowest threshold of macro-pores (0.1 µm). Correspondingly, the proportion of micro-pores in these cores was less than 35% of the total pore volume (Table 4.3). Thus, the ease of percolation in a larger proportion of macro-pores facilitated the absorption and penetrability processes in cores extracted from the regional roads.

Table 4.3: Mercury intrusion porosimetry (MIP) test results for field cores

	Apparent total porosity (%)	**Threshold pore diameter (µm)**	**Proportion of micro-pores (<0.1 µm) (%)**
Residential street I	13.2	0.21	47.1
Residential street II	12.4	0.14	53.2
Regional road I	18.7	2.12	35.4
Regional road II	21.2	3.89	32.4

4.3. Air void system

Performance of concrete subjected to F/T environments is a function of the air void system. Therefore, the quality of the air void system in terms of air content, spacing factor and specific surface area was determined (Table 4.4). Generally, the majority of the concrete cores obtained from joints in regional roads showed lack of air voids dispersed in the paste (Fig. 4.6a). For example, the total air content for these cores was approximately 2.5% which did not satisfy the limits (6.5% ±1.5%) specified by North American codes for durable concrete to F/T cycles (CSA 2014; ACI 201.2R. 2016). Likewise, the key parameter of spacing factor (dispersion of air voids in the cementitious matrix) was significantly higher than that required by these codes (Table 5). Also, the marked drop in the specific surface area (the average air voids size) for the concrete extracted from the regional roads indicated that a significant amount of the smaller air voids diminished. This trend linked to the increase of the threshold pore diameter obtained from the MIP test (Table 4.3). Comparatively, the air void system in the residential streets did not appear to be affected (Fig. 4.6b). Adequate air content (an average of 5.4%), uniform spacing factor (an average of 0.1 mm) and high specific surface area were obtained for this concrete.

Table 4.4: Air void system characteristics for field cores

	Totalaircontent(%) (Target: 5%-8%)	**Spacingfactor (mm) (Target: < 0.2 mm)**	**Specificsurface area (mm^2/mm^3) (Target: > 25 mm^2/mm^3)**
Residential street I	5.29	0.12	49
Residential street II	6.13	0.10	57
Regional road I	3.16	0.48	12
Regional road II	2.43	0.61	9

Note: The results are the average of four samples or more in each area.

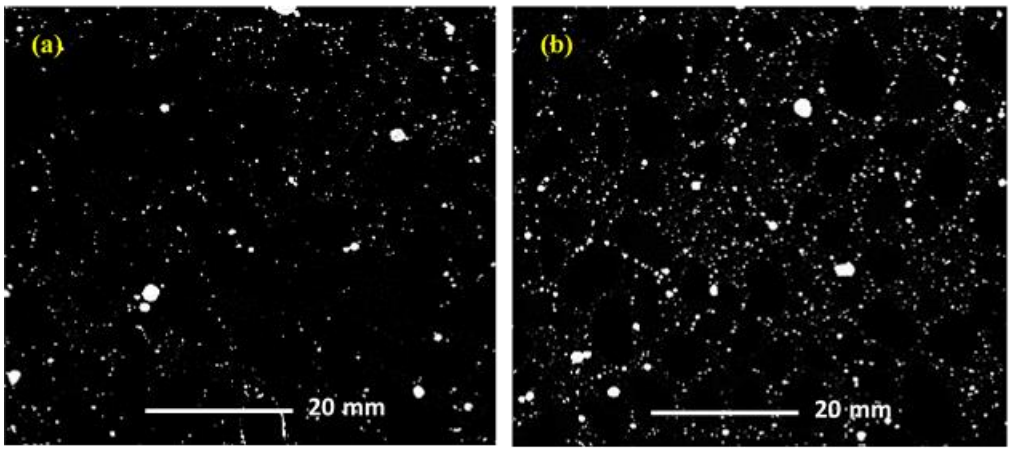

Figure 4.6: Images of polished surfaces treated with wollastonite (white spots) for: (a) regional roads, and (b) residential streets.

4.4. Mineralogical, thermal and microstructural analyses

To characterize the microstructure of this concrete, XRD analysis was performed on powder samples collected from the cores and the results are shown in Fig. 4.7. Also, the XRD pattern for newly (28 days) cast concrete pavement in Winnipeg was used as a reference for identifying possible leaching and new crystalline reaction products. Almost all samples had generally similar dominant phases of quartz, dolomite and calcite. The sources of quartz in the diffractograms originated from the siliceous coarse aggregate and sand, while the peaks of dolomite and calcite occurred because the coarse aggregate contained a fraction of carboniferous aggregate in addition to possible carbonation of the hydrated cement paste.

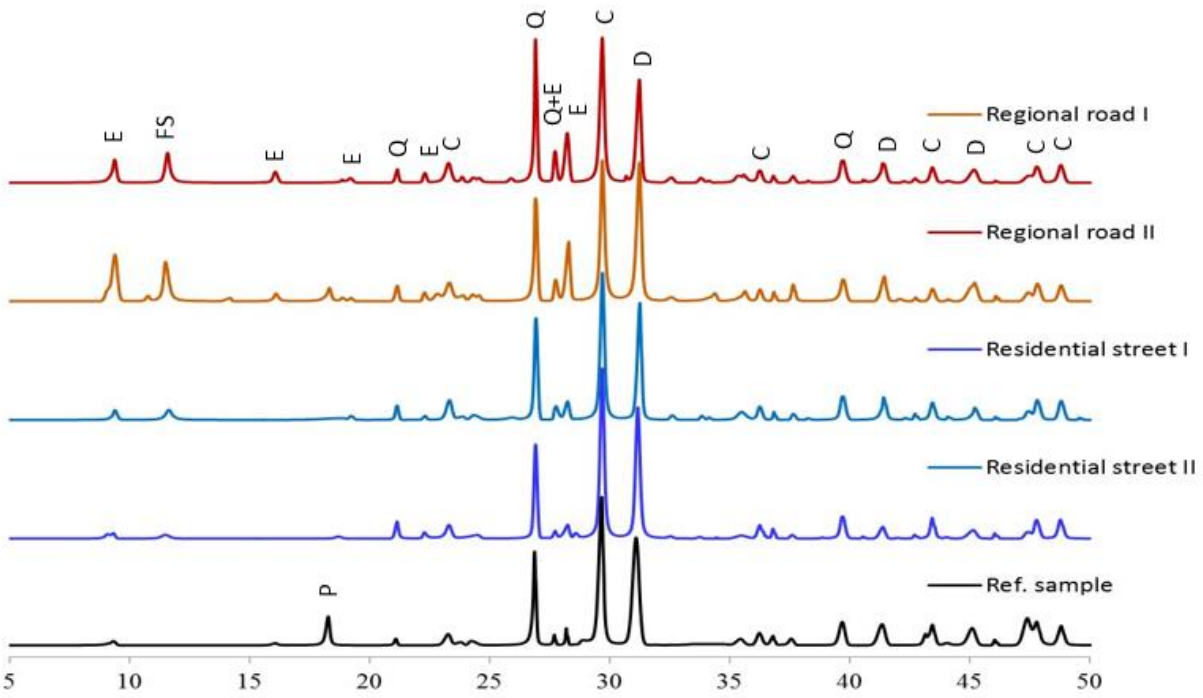

Figure 4.7: XRD patterns of samples from different roads. (Note: E = Ettringite, FS =Friedel's salt, P = Portlandite, D = Dolomite, C = Calcite, and Q = Quartz)

Compared to the reference sample, samples collected from the residential streets generally showed similar XRD patterns, except that portlandite ($Ca(OH)_2$) peaks diminished (Fig. 4.7). Traces of Friedel's salt and ettringite were also noted in some samples. These trends were further corroborated by DSC tests, as shown in Table 4.5. A semi-quantitative analysis based on the enthalpy concept (integration of heat flow peaks over temperature) can determine the relative phase formation, as the enthalpy of each phase (i.e., ettringite, Friedel's salt, portlandite) is directly related to its amount (Brown 1998). The consumption of portlandite in these samples might be due to the long-term pozzolanic activity as this concrete comprised 15 to 20% Type F fly ash and/or leaching/reaction of this phase. However, the bulk properties of concrete from residential streets substantiate the first hypothesis (pozzolanic activity), as this concrete had low absorption, limited penetrability/diffusivity and an effective air void system. Also, the microscopy analysis supported this trend as homogenous matrix without micro-cracks was

observed in various specimens (e.g. Fig. 4.8a), with incidental occurrence of Friedel's salt and ettringite crystals (e.g. Fig. 4.8b) in some voids near (within 10 mm) the exposed surface. The presence of Friedel's salt is likely a result of the substitution of sulfate ions by chloride ions (i.e. chloride binding) in aluminate phases such as monosulfate and unreacted tri-calcium aluminate, if any; however, this phase may not be detrimental to the integrity of concrete as no marked symptoms of cracking and softening were detected.

Table 4.5: Enthalpies (J/g) of the main phases in the cementitious matrix

	Ettringite (90-110°C)	**Friedel's salt (340-390°C)**	**Portlandite (410-450°C)**
Reference sample	5.7	0.0	17.2
Residential street I	8.2	3.6	0.9
Residential street II	6.3	2.9	1.7
Regional road I	39.7	11.9	0.0
Regional road II	48.9	14.2	0.0

Note: The enthalpies results are the average of eight samples or more in each street.

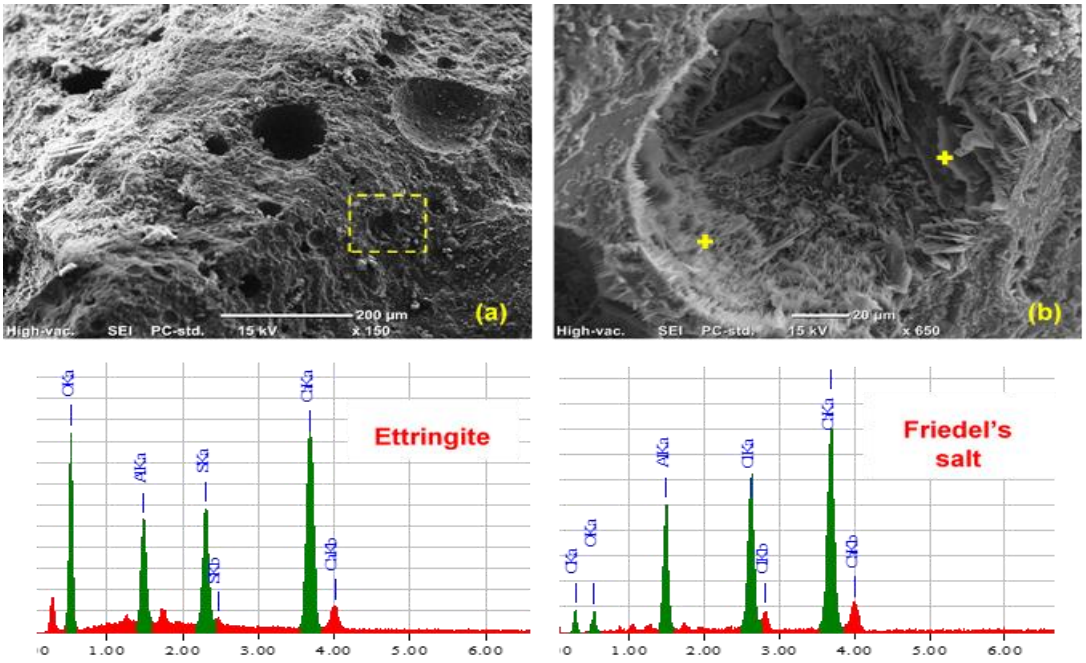

Figure 4.8: Samples collected from residential street showing: (a) homogenous and dense matrix; and (b) traces of Friedel's salt and ettringite crystals precipitating in air voids with associated EDX spectra.

Conversely, samples extracted from the regional roads showed distinctive XRD pattern, as shown in Fig. 4.7. Higher intensity peaks of ettringite and Friedel's salt were detected in this concrete as the key reaction products. This trend was further supported by the DSC analysis; for instance, Table 6 shows that the amounts of ettringite and Friedel's salt formed in the regional roads samples were approximately 7 and 4 times, respectively that in the residential streets samples. SEM showed that this concrete had high intensity of micro-cracks (e.g. Fig. 4.9a) and most air voids (both small and large) were filled with various levels of secondary depositions (e.g. Fig. 4.9b). Spatial elemental distribution by EDX revealed that the secondary depositions were mostly ettringite (e.g. Fig. 4.9c). This observation complies with previous studies on field performance of concrete pavements (Ranjaraju 2002; Arribas-Colón et al., 2012) which reported the presence of secondary depositions in the cementitious matrix. The more formation of Friedel's salt can be attributed to the higher availability of chloride ions at these locations due to chloride binding, as discussed earlier, while re-crystallization and/or new formation of ettringite might be attributed to different reasons (availability of the components that form ettringite, Ostwald ripening, variations in pH and temperature). First, if external (e.g. as impurities in de-icing salts, or dissolved in ground water) or internal (e.g. from aggregates) sources of sulfate ions are present, the sulfate would react with monosulfate to form ettringite with consequent deposition in open spaces, such as air voids. However, if no sources of sulfate are available, ettringite may form due to repetitive saturation in the system (W/D and F/T cycles), which may induce expansion due to its formation (Stark and Bollmann 1999). However, it is not certain whether the growth of larger secondary ettringite in air voids is expansive, as expansive damage of paste is usually attributed to micro-crystalline ettringite formed in the hydrated paste (Mather 2001; Skalny et al., 2002). Detwiler and Powers-Couche (1999) reported that expansion and

distress of pavements in Wisconsin occurred before much ettringite deposited in air voids. Ouyang et al., (1999) and Famy et al., (2001) stated that ettringite found in this benign state as large needle-shaped or compact crystals (Fig. 4.9b), should not necessarily be interpreted as the cause of damage of concrete since this may be just a consequence of re-crystallization. Johansen et al., (1995) stated that ettringite formation in microstructural defects can be promoted by frequent drying and repeated wetting. They stated that the higher the amount of water passing into the capillary system, the higher the apparent amount of ettringite was observed (Johansen et al., 1995). Indeed, such moisture conditions were available in the wet joint of regional roads. Small crystals (with higher specific surface and surface energy) dissolve in the pore solution and recrystallize as large crystals in available large spaces, such as pores and cracks [Ostwald ripening] (Stark and Bollmann 1999). Whether ettringite crystals formed in air voids are expansive or not, in-filling of air voids (especially smaller air voids) with secondary products reduced their effectiveness (inadequate air-void system; Table 4.4 and Fig. 4.6) to providing an adequate level of F/T protection. In-filling of air voids with ettringite or any precipitates in concrete from regional roads may also ease reaching critical saturation levels due to higher rates of moisture ingress (Fig. 4.4) because the air voids are not available anymore to interrupt the paths of penetrability (Stark and Bollmann, 1999). This made this concrete vulnerable to progressive F/T damage as manifested by micro- and macro-cracking and eventually crumbling (Fig. 4.2). Moreover, holding solution (due to the application of de-icing salts) in these joints further increased the degree of saturation as salt solutions have lower vapor pressure than that of pure water (Mehta and Monteiro, 2014). These trends suggest that concrete at joints in regional roads might have suffered from F/T cycles as the primary mechanism of deterioration.

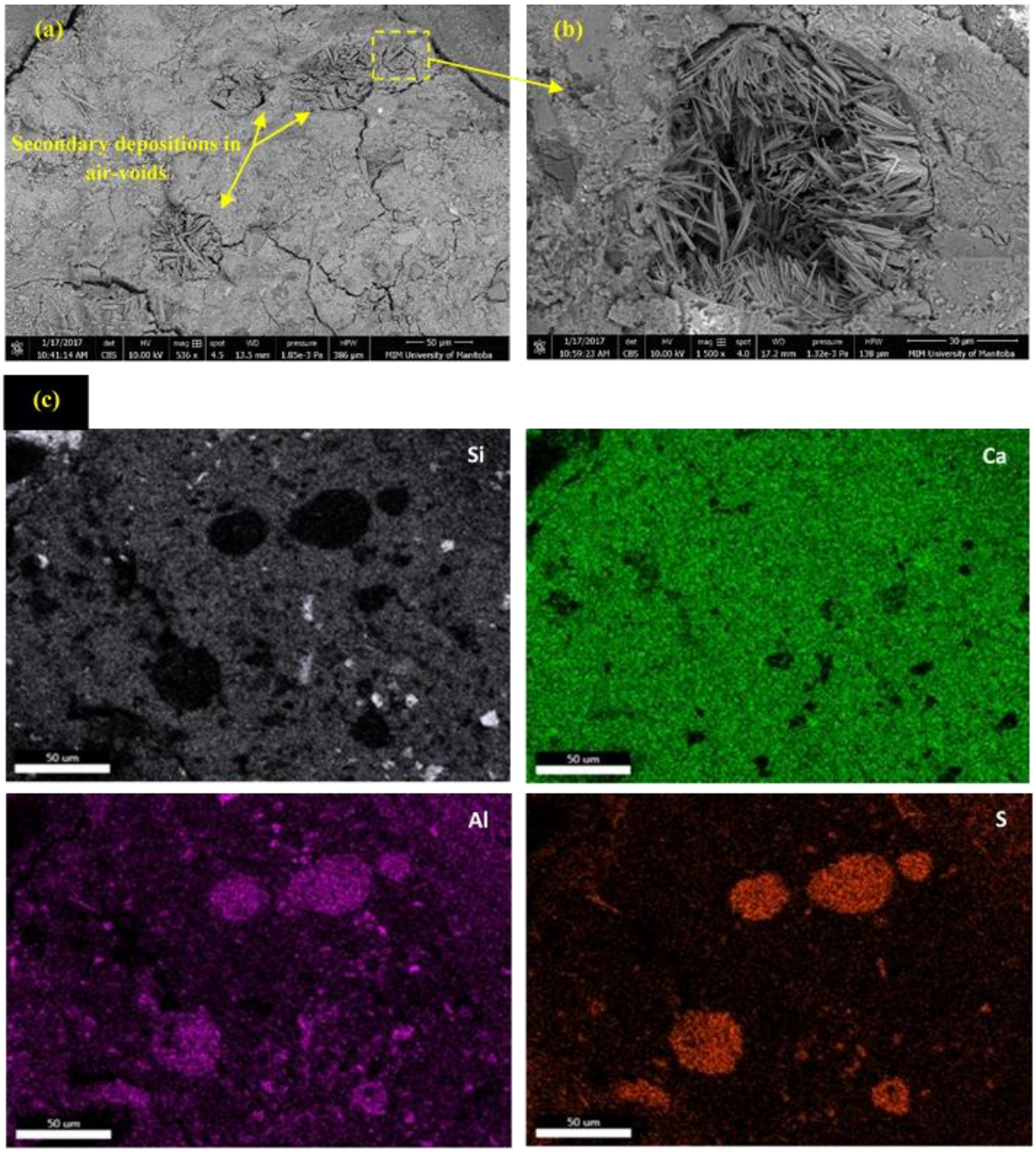

Figure 4.9: Example of microanalysis for a specimen from regional roads showing: (a) high intensity of micro-cracks, (b) secondary depositions filling air-voids, and (c) elemental spatial distribution for the field of view in (a).

5. Results and Discussion of the Laboratory Study

5.1. Rapid Chloride Penetrability Test

The penetrability of all the reference, binary and ternary mixtures was evaluated by the Rapid Chloride Penetrability Test (RCPT) at day 28. At the end of RCPT, the physical penetration depth of all the prepared mixtures was measured by splitting the concrete specimens in half and spraying silver nitrate ($AgNO_3$) solution. The whitish precipitate of silver chloride indicating the penetration depth of chloride ion was clearly visible as shown in Fig. 5.1. The results of passing charges, chloride ion penetrability class according to ASTM C1202 and average physical penetration depth obtained from the test are presented in Table 5.1. It's worth mentioning that, the trend of passing charges and penetrability class is consistent with the penetration depth results, where the higher passing charges correspond to higher penetration depth and vice versa.

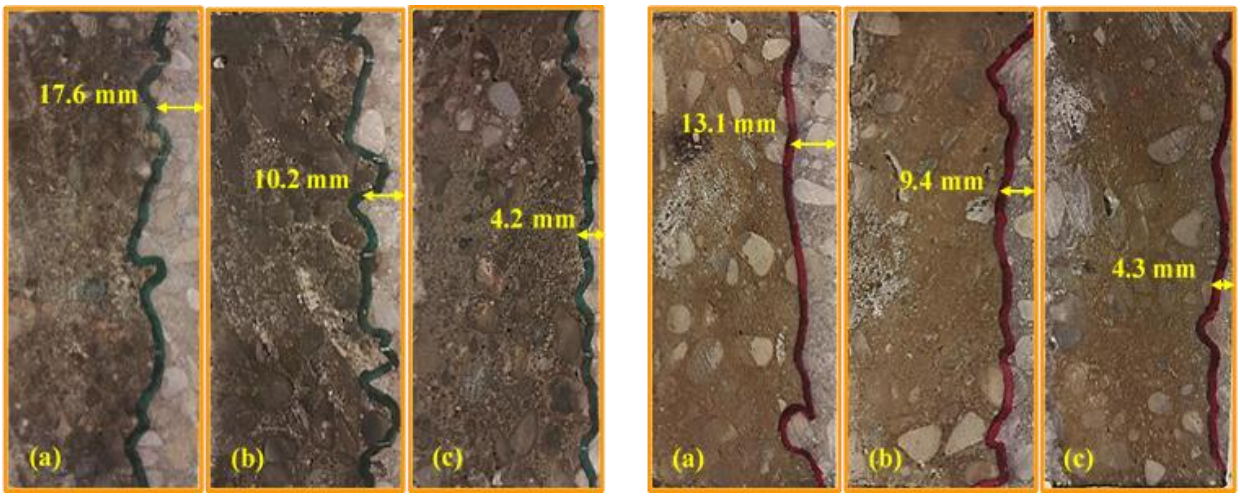

Figure 5.1: Whitish precipitate showing the average penetration depth of chloride ions in specimens (GU at left and PLC at right) (a) single binder, (b) binary binder (30% fly ash) and (c) ternary binder (30% fly ash with nanosilica).

Table 5.1 RCPT results

Mixture ID.	Charges Passed (coulombs)	Chloride Ions Penetrability Class (ASTM C1202)	Average Penetration Depth (mm)	Standard Error of Penetration Depth
GU group				
GU	2248	Moderate	17.6	0.94
GUF20	1527	Low	12.8	0.64
GUF30	1253	Low	10.1	0.57
GUS	743	Very Low	5.2	0.6
GUF20S	716	Very Low	5.1	0.73
GUF30S	463	Very Low	4.2	0.64
PLC group				
PLC	1867	Low	13.1	1.07
PLCF20	1470	Low	11.4	1.14
PLCF30	917	Very Low	9.4	0.96
PLCS	871	Very Low	6.3	0.81
PLCF20S	347	Very Low	4.6	0.38
PLCF30S	475	Very Low	4.3	0.53

The PLC has higher fineness (460 m^2/kg) than the reference GU cement (390 m^2/kg) as PLC contains inter-ground limestone powder with clinker. Incorporation of additional limestone is expected to improve the cement hydration process and the continuous particle size distribution resulting in filler effect and better particle packing in the matrix (Ramezanianpour and Hooton, 2014). Thus, the RCPT test conducted in this study exhibited microstructural improvement in PLC concrete by reducing the penetration depth by about 26% relative to reference GU mixture. However, this observation was completely diminished for all other mixtures (binary and ternary) due to the predominant effect of used SCMs and nanoparticles. In general, the incorporation of fly ash and nanosilica had a significant improvement in both GU and PLC concrete microstructure and had comparable significant effect in reducing the penetration depth (Table 5.1). Incorporation of higher percentage of fly ash reduced the penetrability of concrete but with much improvement in the microstructure with the addition of nanosilica particles. For instance, the binary (GUS) and ternary (GUF30S) mixes containing nanosilica reduced about 70% and 76% of chloride penetration depth relative to reference GU mixture. The same observation was

made in case of all PLC group binary and ternary mixtures. Effects of this improved microstructure were clearly reflected on the performance of mixtures tested in this study which are presented in subsequent sections.

5.2. Visual Assessment

Regular visual observation was made prior to any measurements to assess the effects of freeze-thaw (F/T) action on the specimens. The overall observation revealed an excellent condition of most of the specimens without any features of damage. The NaCl salt solution seemed to be benign towards all specimens, without detrimental effects up to 600 F/T cycles (Fig. 5.2). In the case of $MgCl_2$ solution, only the reference GU sample showed signs of damage. Surface deterioration and loss of aggregates accompanied by longitudinal cracks were the main feature of deterioration in these specimens (Fig. 5.3). On the other hand, the binary and ternary mixture specimens showed excellent resistance to F/T action and no visible deterioration was observed (Fig. 5.3).

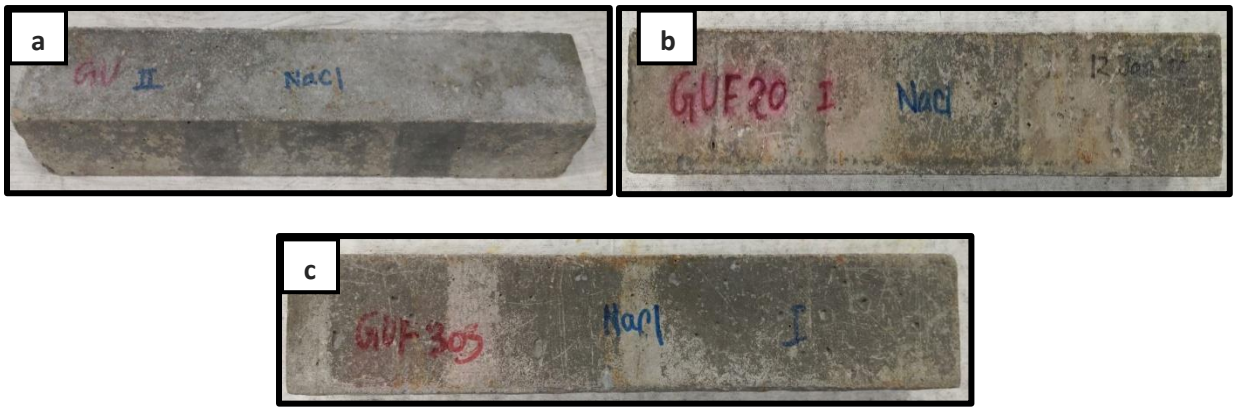

Figure 5.2: Sound specimens exposed to the NaCl solution after 600 F/T cycles: (a) single (GU) (b) binary (GUF20), and (c) ternary (GUF30S) binders.

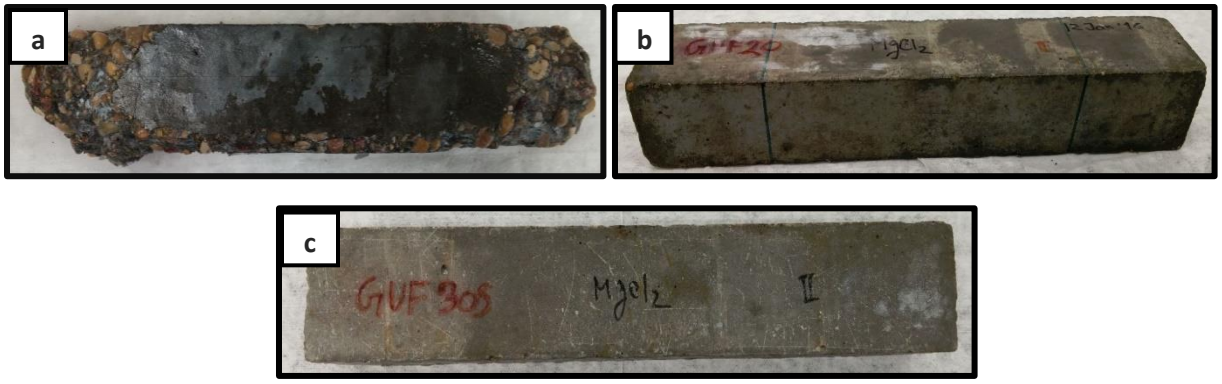

Figure 5.3: Specimens exposed to the $MgCl_2$ salt solution: (a) deteriorated GU after 476 cycles and intact (b) GUF20 and (c) GUF30S specimens after 600 cycles.

The $CaCl_2$ solution was more aggressive than the $MgCl_2$ solution in this F/T exposure. The reference GU and binary mixtures (20% fly ash) in the $CaCl_2$ solution started to lose paste from the surface after 168 cycles and 224 cycles, respectively and eventually both the mixtures suffered severe surface scaling (Fig. 5.4). The rest of the binary and ternary mixtures containing nanosilica and higher dosage of fly ash (30%) in this solution showed resistance against any visible damage up to 600 cycles (Fig. 5.5).

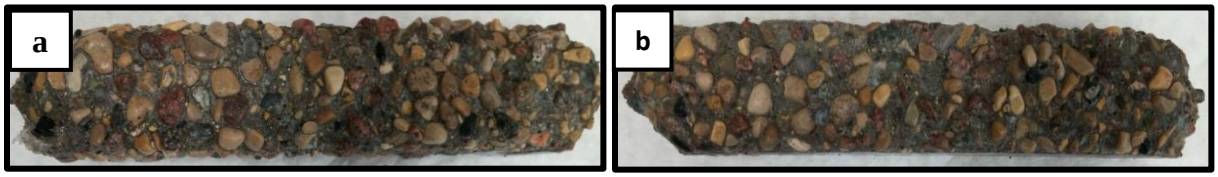

Figure 5.4: Reference and binary mixture specimens exposed to the $CaCl_2$ solution: (a) GU after 392 cycles, and (b) GUF20 after 476 cycles.

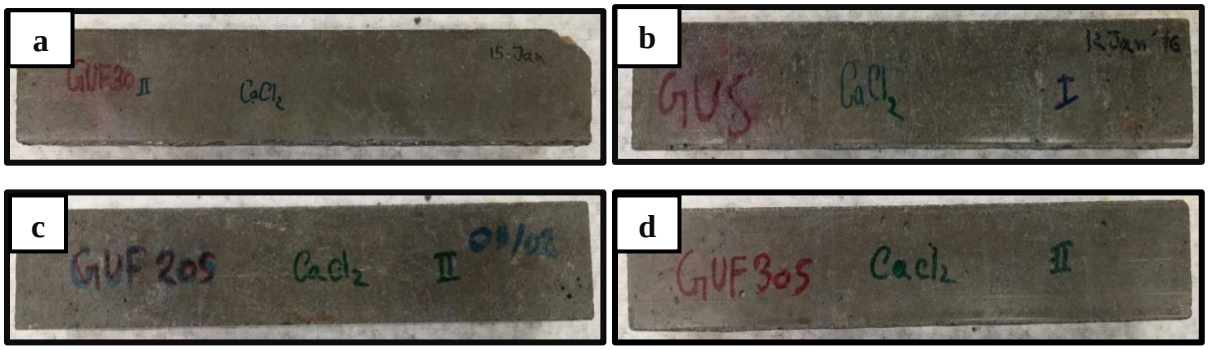

Figure 5.5: Intact specimens exposed to the $CaCl_2$ solution after 600 cycles: (a) GUF30, (b) GUS, (c) GUF20S and (d) GUF30S.

On the other hand, PLC and PLCF20 specimens in the $CaCl_2$ solution showed paste loss from the surface (Fig. 5.6). Although, these specimens suffered moderate surface scaling, they completed 600 F/T cycles without any further visible damage. Except these two mixtures, all other PLC mixture specimens in the $CaCl_2$ solution showed good resistance to this exposure. The other salt solutions were not aggressive towards any PLC mixture as specimens were in sound conditions at the end of the F/T regime.

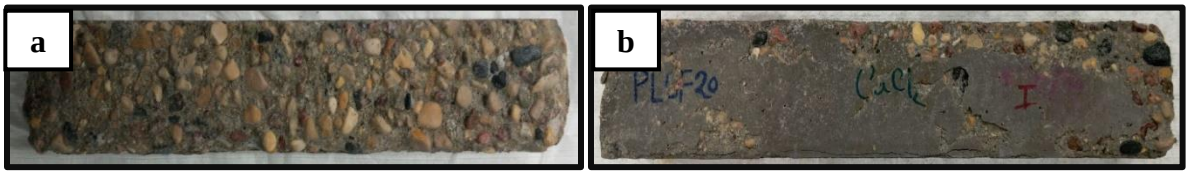

Figure 5.6: Deteriorated (a) PLC and (b) PLCF20 specimens exposed to the $CaCl_2$ solution at the end of F/T regime.

5.3. Mass Loss

The values obtained during the mass loss measurement corresponded to the visual observations made over the F/T exposure period. Figure 5.7 shows the mass change of all GU specimens in the three different salt solutions over the entire F/T exposure. For instance, every specimen kept in the NaCl solution had no mass loss, instead experienced a steady mass gain over time. The GU and GUF 20 specimens in the $CaCl_2$ suffered a significant mass loss of 31% and 26% respectively before failing. They started exhibiting signs of deterioration by losing paste from the surface and splitting in half after 392 cycles (GU) and 476 cycles (GUF20), respectively. Comparatively, the reference GU specimens failed after 476 cycles in the $MgCl_2$ solution with a mass loss of 14%. Generally, the binary and ternary mixtures containing SCM and nanoparticles showed excellent resistance to this severe F/T exposure. All other binary and ternary mixtures subjected to $MgCl_2$ and $CaCl_2$ salt solutions experienced a steady mass gain (maximum of 1%) with time.

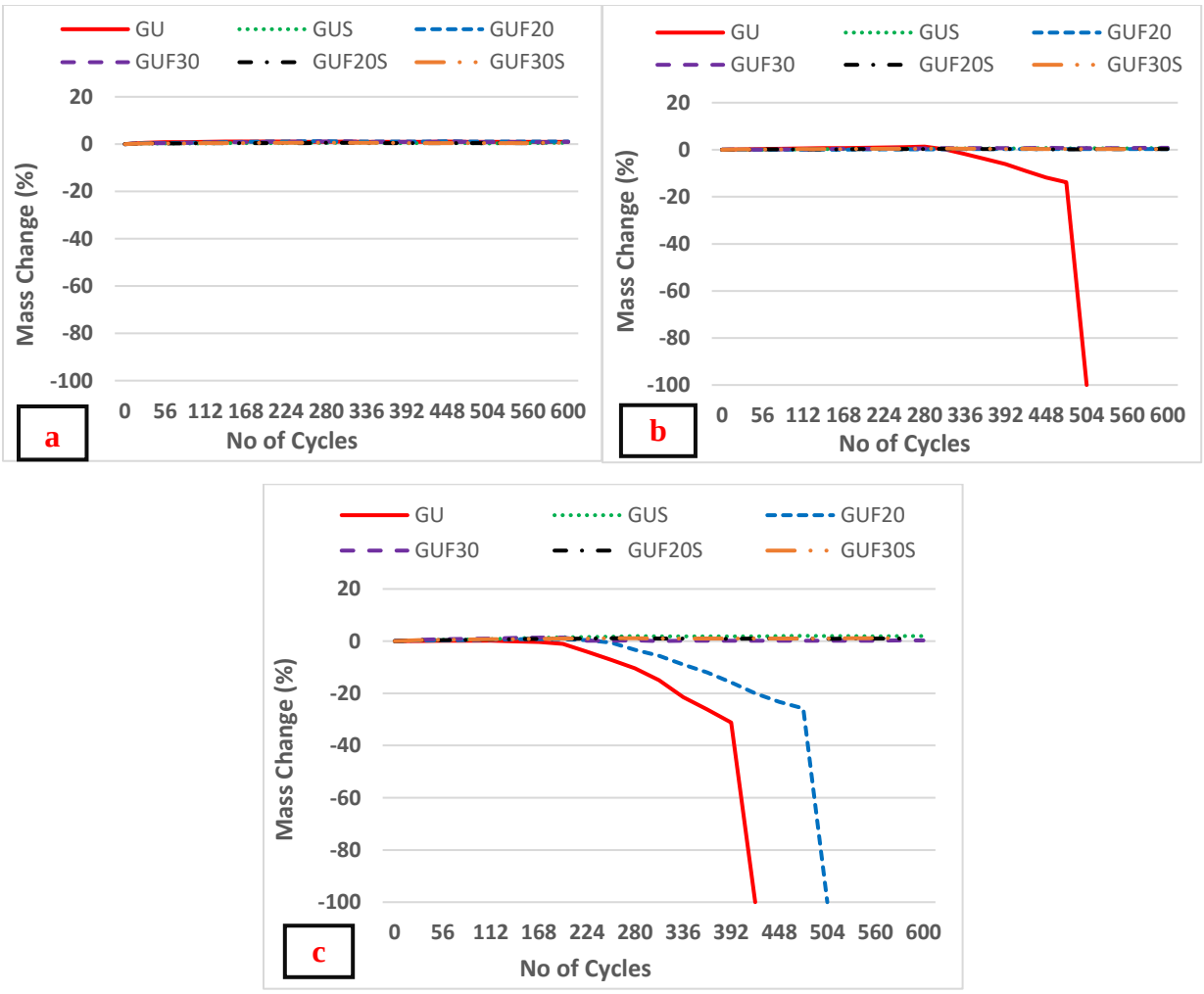

Figure 5.7: Mass change vs. the time of F/T exposure for all GU group specimens exposed to (a) NaCl (b) $MgCl_2$ and (c) $CaCl_2$ salt solutions.

On the other hand, the $CaCl_2$ solution proved to be aggressive for PLC samples as well. The PLC and PLCF20 specimens in this salt solution encountered some mass loss due to moderate surface scaling. The PLC specimens had a slight mass loss of 7% and the PLCF20 specimens also experienced a mass loss of 6% (Fig. 5.8). Except for these two binders in the $CaCl_2$ solution, the rest of the PLC specimens in all salt solutions had a similar pattern of gradual mass gain (less than 1%) like the GU group specimens over the entire period of exposure.

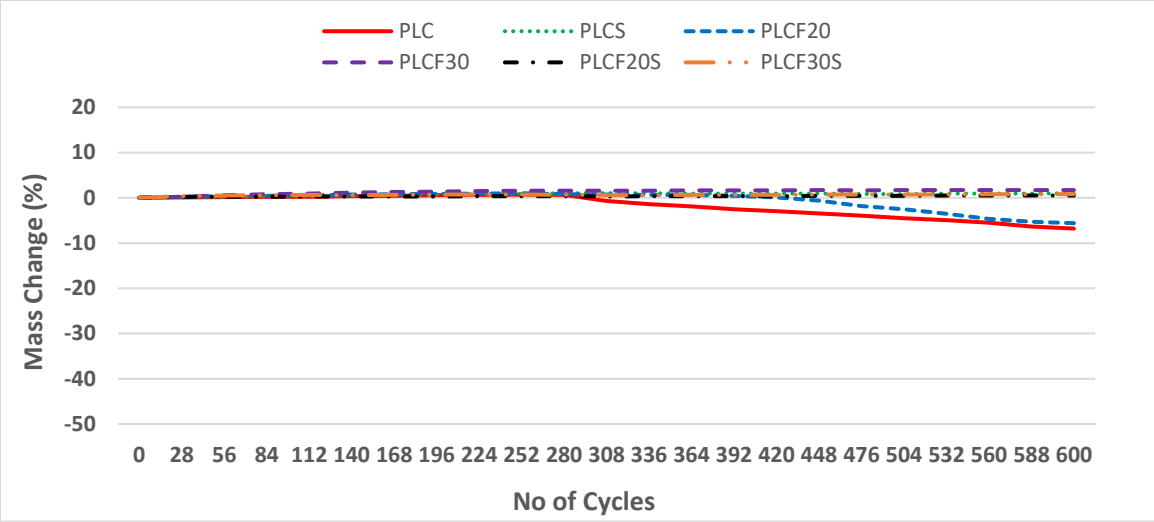

Figure 5.8: Exemplar mass change vs. the time of F/T exposure for the PLC group specimens exposed to the $CaCl_2$ solution.

5.4. Length Change

Almost all specimens exposed to the F/T conditions in different salt solutions had no significant length change. The length change observation result for all the GU and PLC mixtures sample is shown in Fig. 5.9. All the GU and PLC group specimens exposed to the NaCl solution had negligible expansion (maximum 0.05%). As the specimens showed no signs of damage and had regular reaction products in the matrix (as shown later in the XRD analysis). Therefore, the specimens in this exposure showed almost a constant value in the length change over the entire exposure period (Fig. 5.9). Specimens in the $MgCl_2$ solution had similar trends in terms of length change except for the reference GU specimens. Up to 336 cycles, these specimens had negligible (0.03%) expansion, but afterwards it experienced a drastic gradual expansion (up to 0.15%) before failure. This can be ascribed to the nature of degradation (chemical deterioration as discussed in XRD and SEM sections). Although during the visual inspection and mass loss observations, the $CaCl_2$ salt solution was shown to be the most aggressive salt, but in terms of the length change, specimens in this solution had negligible expansion (maximum .032%).

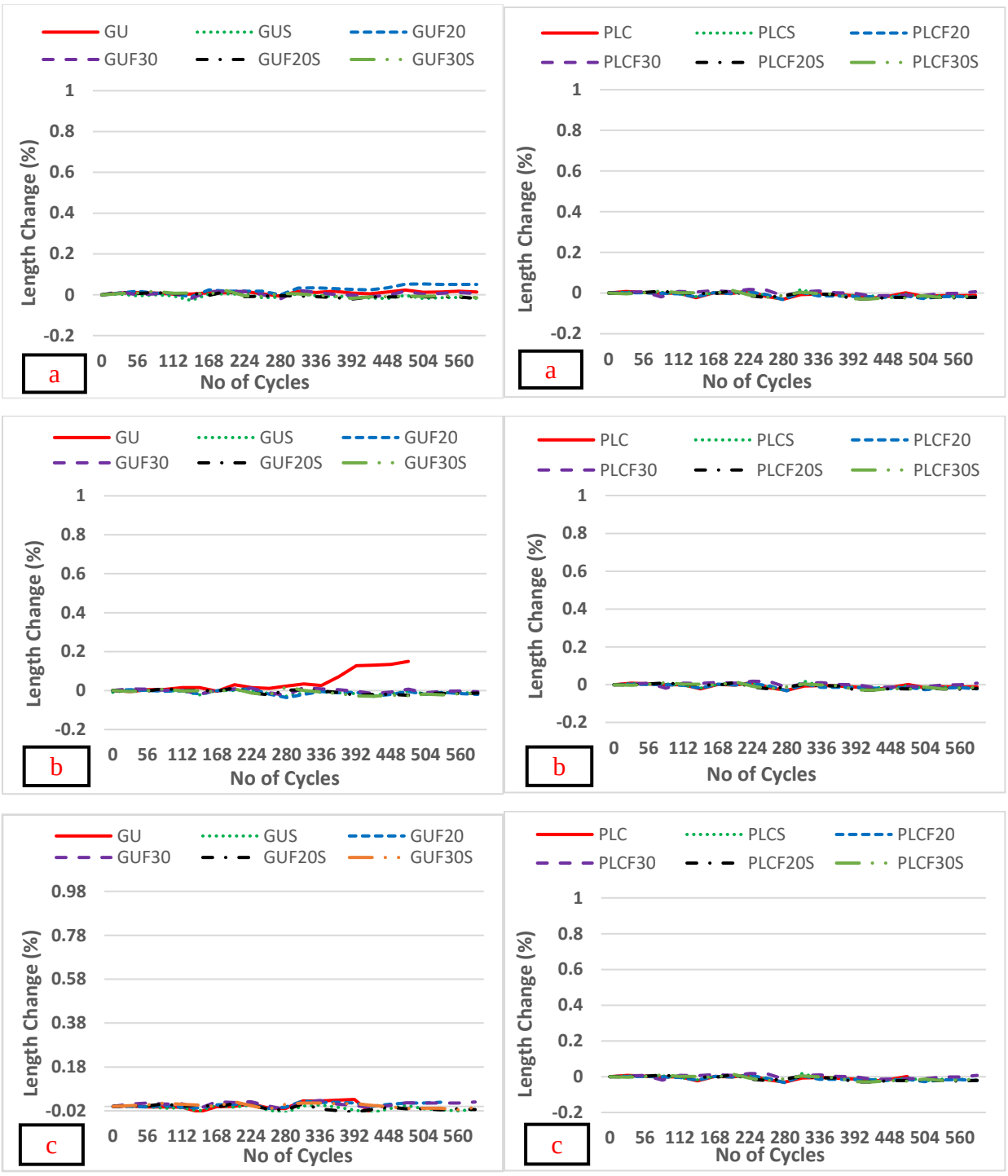

Figure 5.9 Length change vs the time of F/T exposure for all GU mixture specimens (GU at left and PLC at right) exposed to (a) NaCl, (b) $MgCl_2$ and (c) $CaCl_2$ salt solutions.

5.5. Relative Dynamic Modulus of Elasticity (RE_d)

The relative dynamic modulus of elasticity (RE_d) of the specimens was measured to capture any internal damage of concrete specimens due to the F/T action (Fig. 5.10). Similar to the previous trends, no single specimen in the NaCl salt solution showed reduction in RE_d values up to the end of exposure period. This indicates an undamaged microstructure and better resistance against any F/T action for all the specimens exposed to the NaCl salt solution. However, few mixtures exposed to the $CaCl_2$ showed inferior resistance against the detrimental effects of F/T action. The GU and GUF20 specimens had undergone gradual reduction in RE_d values similar to the mass loss trends. Before showing zero RE_d at failure, the GU and GUF20 samples had almost 19% and 16% reduction of RE_d values, respectively. Unlike the mass loss experience, the GU specimen in the $MgCl_2$ solution had much higher reduction (almost 32%) of RE_d before failure. This higher percentage of reduction in RE_d corresponded to significant internal cracking in addition to the outside cracks observed during visual inspection. No other mixture samples in these salt solutions had reduction in RE_d through out the entire F/T exposure.

The PLC group specimens also showed better resistance to any kind of internal damage caused by F/T action. Most of the specimens had almost constant RE_d values throughout the whole exposure period. Only the PLC and PLCF20 specimens in the $CaCl_2$ solution experienced reduction in RE_d. The progressively moderate scaling at the surface might have instigated some internal damages which were captured in the RE_d observations, but the reduction of RE_d was not significant with an average of 7%. The overall trends of RE_d indicate compearable performace of PLC mixtures in the F/T exposure.

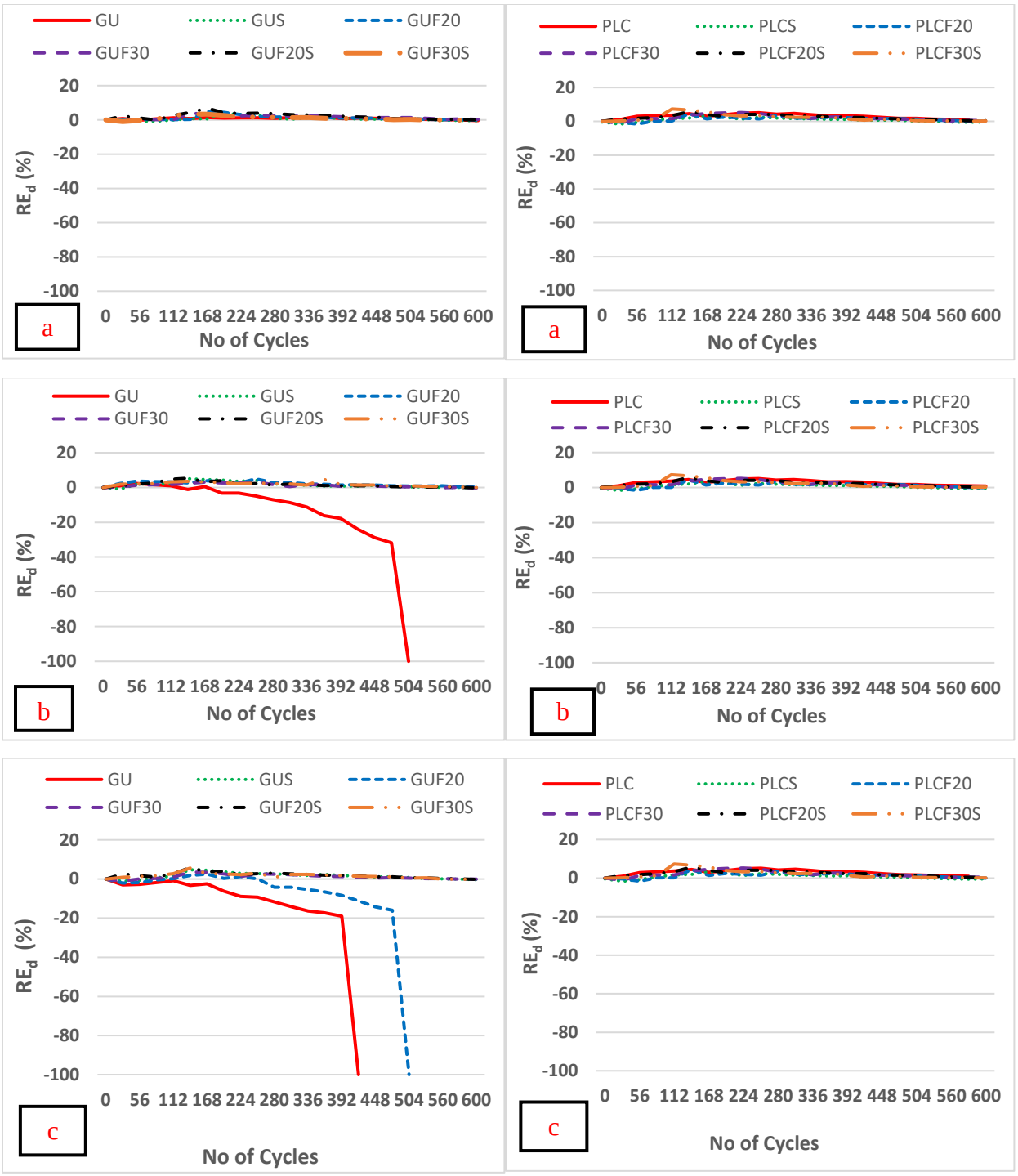

Figure 5.10: RE_d vs. the time of F/T exposure for GU (left) and PLC (right) group specimens exposed to: (a) NaCl, (b) $MgCl_2$ and (c) $CaCl_2$ salt solutions.

5.6. Mineralogical, Thermal and Microstructural Analyses

To detect the underlying mechanisms of damage, XRD analysis was conducted on powder samples collected from the surface of selected specimens (Single binder: GU and PLC, binary binder: GUF20 and ternary binder: GUF30S), and the results are shown in Figs. 5.11-5.13. The XRD patterns generally showed similar dominant phases of dolomite, quartz and calcite. A fraction of carboniferous coarse aggregate is most likely the reason behind the peaks of dolomite and calcite. The sources of quartz in the diffractograms originated from the siliceous coarse aggregate and sand in all the mixtures as well as fly ash in some binders.

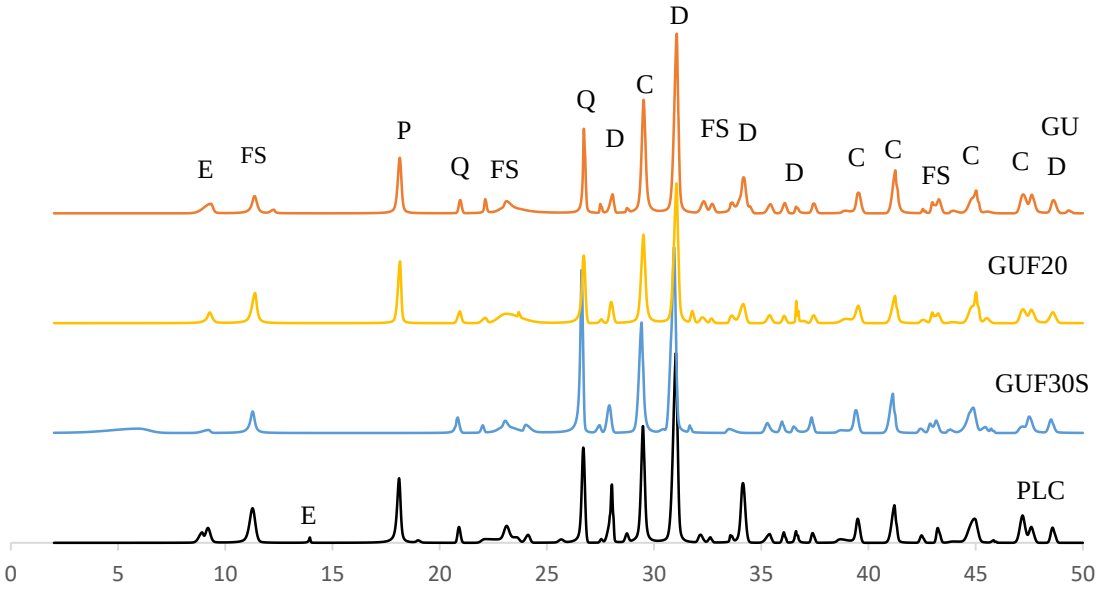

Figure 5.11: XRD patterns of specimens exposed to the NaCl solution. (Note: E= ettringite, FS= Friedel's salt, P= portlandite, Q= quartz, D= dolomite, C= calcite)

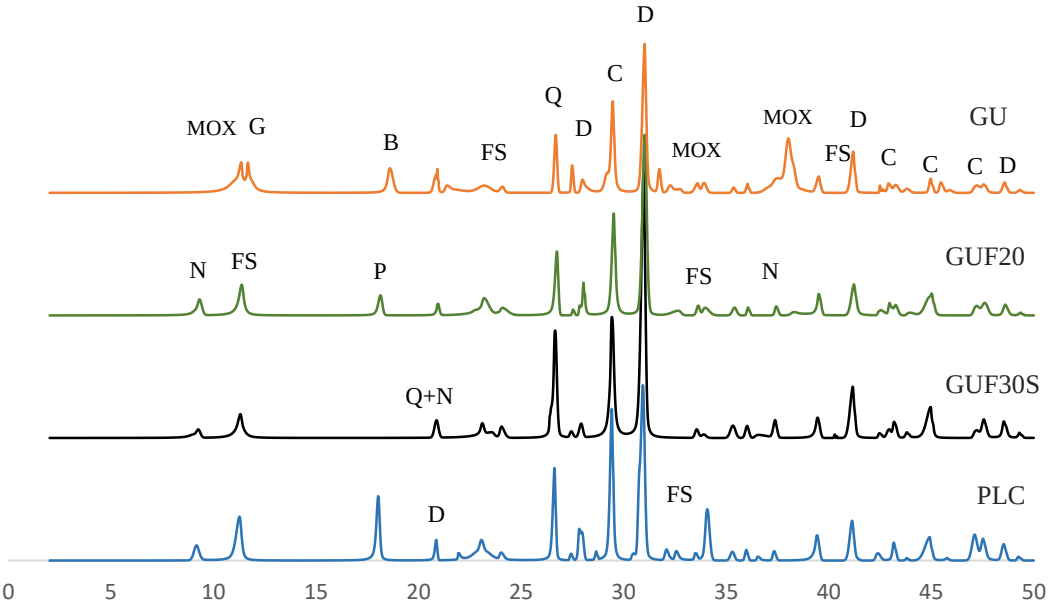

Figure 5.12: XRD patterns of specimens exposed to the $MgCl_2$ solution. (Note: MOX= magnesium oxychloride, G= gypsum, N= nepskoeite, B= brucite FS= Friedel's salt, P= portlandite, Q= quartz, D= dolomite, C= calcite)

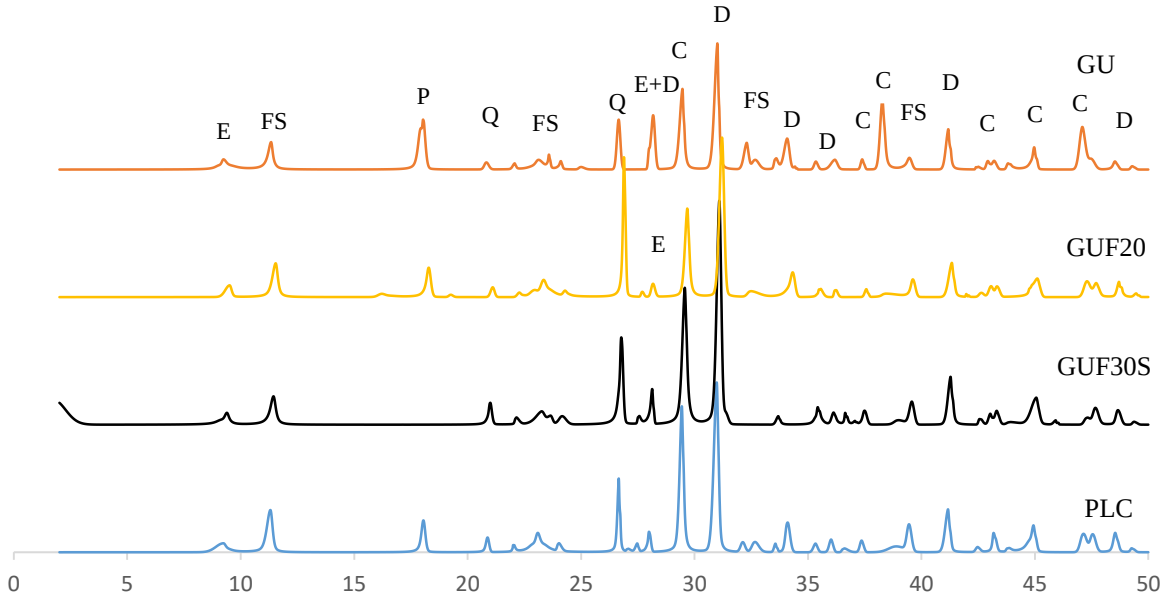

Figure 5.13: XRD patterns of specimens exposed to the $CaCl_2$ solution. (Note: E= ettringite, FS= Friedel's salt, P= portlandite, Q= quartz, D= dolomite, C= calcite)

At low concentration 3-5% NaCl was reported as an aggressive de-icing salt concerning surface scaling of concrete (Valenza and Scherer, 2006; Shi et al., 2010). However, this compound seems to be harmless at higher concentration (14.2%) used in this study, as no signs of deterioration were observed for all specimens in this solution up to 600 cycles of F/T exposure. For all the mixtures, the XRD patterns showed similar dominant phases of calcite, quartz, dolomite, Friedel's salt and ettringite. Portlandite peaks were also identified in all specimens after the exposure except that the mixtures containing nanoparticles (e.g. GUF30S; Fig. 5.11). The depletion of the amount of portlandite in these matrixes was due to dilution of the cement component and increased pozzolanic activity, resulting in production of additional/secondary C-S-H gel, as reflected by the matrix densification observed in the RCPT results (Table 5.1). The presence of Friedel's salt is likely because of the substitution of sulfate ions by chloride ions (i.e. chloride binding) in aluminate phases such as monosulfate and unreacted tri-calcium aluminate, if any. With time, the releasable sulfate ions combine with the remaining monosulfate and a part of Friedel's salt already formed, precipitating ettringite, as substantiated by higher intensity of ettringite peaks in Fig. 5.11. These phases may not be detrimental to the integrity of concrete as no marked symptoms of cracking and scaling were detected (Fig. 5.2 in visual inspection section). The microscopy analysis supported this trend as homogenous matrix without micro-cracks was observed in various specimens (e.g. Fig. 5.14a), with incidental occurrence of Friedel's salt and ettringite crystals (e.g. Fig. 5.1 4b) in some voids near (within 10 mm) the exposed surface.

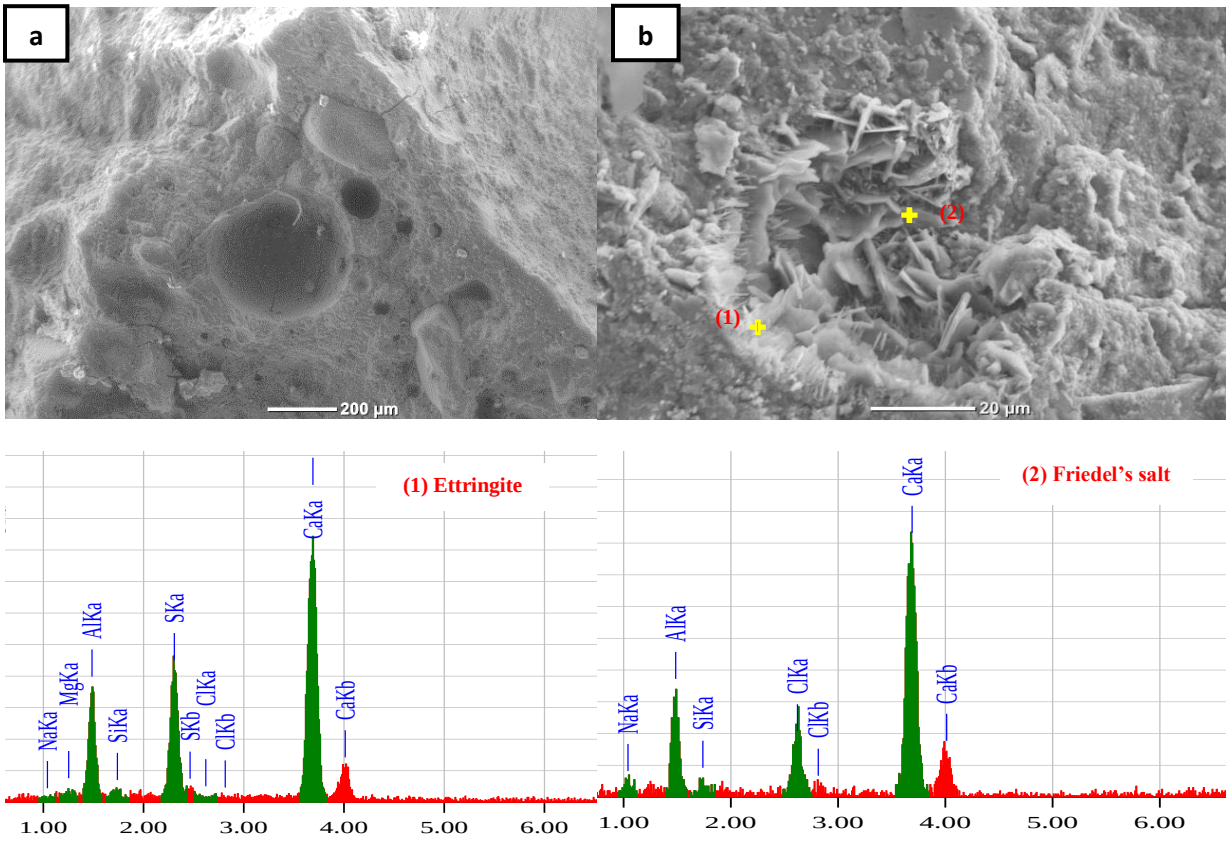

Figure 5.14: Exemplar micrographs of SEM and EDX analyses of a GU specimen in NaCl after 600 cycles showing: (a) homogenous and dense matrix; and (b) traces of Friedel's salt and ettringite crystals precipitating in air voids.

In the $MgCl_2$ solution, the XRD patterns were slightly different than that observed in the NaCl solution, especially the reference GU specimens. Generally, the ettringite peaks were totally diminished in all the samples. This may be attributed to the drop in the pH of the pore solution (~9.5) as ettringite is known to be unstable and dissolves below a pH around 10.7 (Gabrisova et al., 1991). Also, fine peaks of 'Nepskoeite' (N; $Mg_4Cl(OH)_7{\cdot}6H_2O$) was detected for all the specimens immersed in $MgCl_2$ solution. Nepskoeite is a crystalline compound associated with anhydrite $MgCl_2$ salt. The reference GU mixture in the $MgCl_2$ solution suffered chemical degradation under such conditions. Dissolution of portlandite and formation of brucite led to a drop in the pH of the pore solution, resulting in destabilizing ettringite. The releasable sulfate

ions (from monosulfate, or the dissolution of ettringite due to its instability at low pH) react with calcium ions in the pore solution, resulting in gypsum formation, as shown in Fig. 5.12. With time, the saturation of the pore fluid with respect to magnesium, calcium, chloride, and hydroxide ions lead to crystallization of magnesium oxychloride, resulting in expansion (Fig. 5.9 a.) and disintegration of the specimens. These trends were further corroborated by the SEM and EDX analyses, as shown in Fig. 5.15 and 5.16.

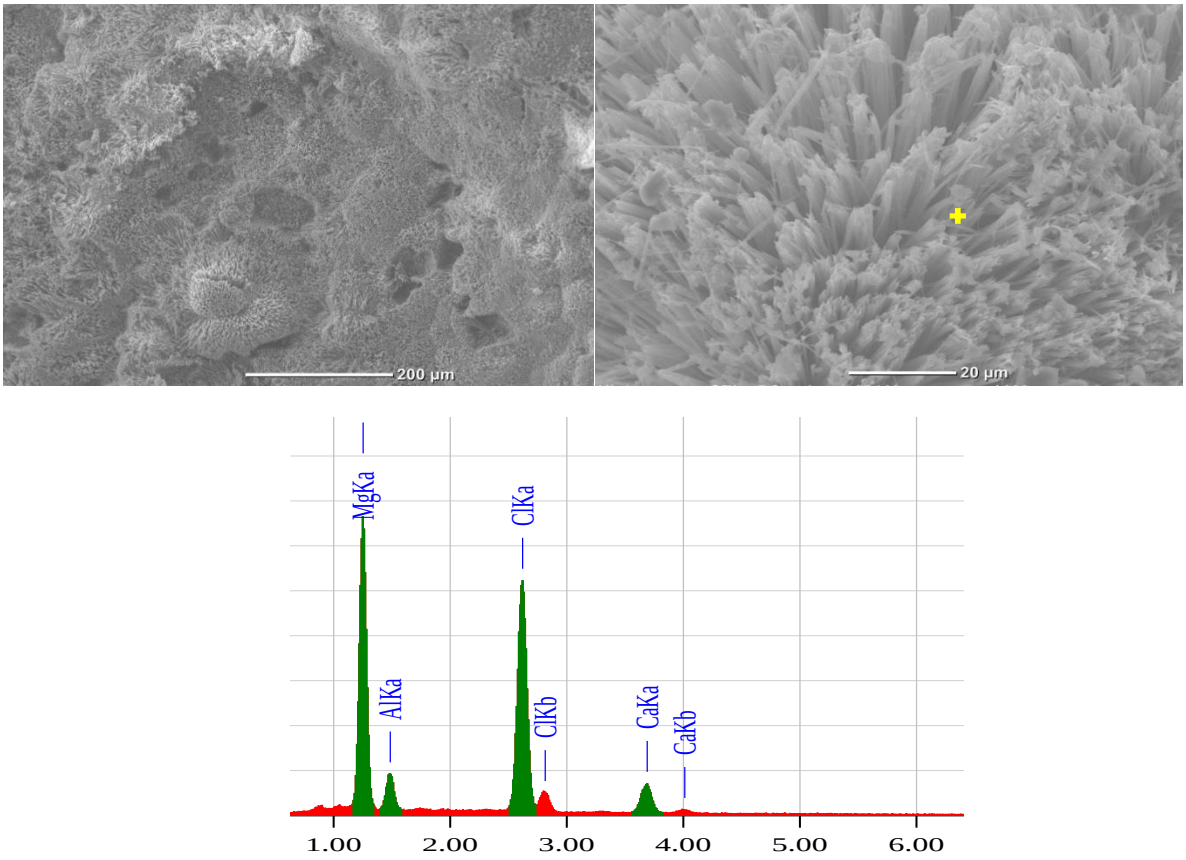

Figure 5.15: SEM micrographs and associated EDX spectra of fracture piece from GU specimen in $MgCl_2$ showing; (**a**) needle-like crystals of magnesium oxychloride growing on the surface, and (**b**)a close-up showing the morphology of the crystals.

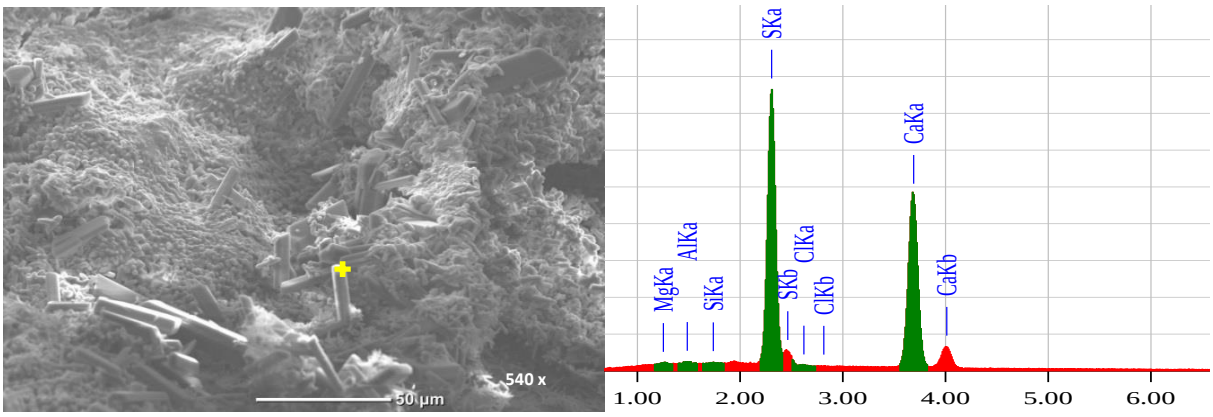

Figure 5.16: SEM micrographs and associated EDX spectra of fracture piece from GU specimen in $MgCl_2$ showing gypsum crystals.

In the $CaCl_2$ solution, the XRD patterns showed similar dominant phases of dolomite, calcite and quartz like the NaCl solution. Although the XRD pattern here is similar but specimens specially the GU and GUF20 in $CaCl_2$ solution suffered severe scaling and failed before 600 F/T cycles. Traces of Friedel's salt and ettringite were also available in specimens in this solution. Reaction between the chloride ions from de-icing salt and the hydration products of aluminate content in cement produced chloroaluminate crystallization (Friedel's salt). But type of cation (e.g. Ca^{2+}, Na^{+} etc.) of chloride salt has effect on the amount of Friedel's salt formation through the binding of chloride ions. Furthermore, almost one and half times more bound chlorides exist when Ca^{2+} cation is present in comparison to Na^{+} (Arya et al., 1990; Delgrave et al., 1997). Higher peaks in Fig. 5.13 indicates formation of larger amount of Friedel's salt in GU and GUF20 specimens subjected to $CaCl_2$ solution and the SEM analysis (Fig. 5.17) confirmed Friedel's salt deposition inside voids. Deposition of this large amount of Friedel's salt in voids created immense pressure on concrete. Again, the required energy to melt ice in presence of de-icing salt is drawn from concrete surface which results in differential strain within the concrete due to a temperature gradient (Sumsion et al., 2013). Due to ice melting capacity at much lower temperature the amount of differential strain in concrete subjected to $CaCl_2$ solution is much higher. Thus, the

combined effect of additional Friedels's salt formation and differential strain might have instigated the observed severe scaling (Fig. 5.4) of concrete in this salt solution. Resistance of any kind of scaling in other samples in this solution especially concrete containing 30% fly ash (GUF30), most probably occurred due to the better physical resistance of these samples against any fluid and ion ingress (Table. 5.1). The lower permeability of the intact mixture samples reduced the amount of available chloride ions to bound inside concrete and thus avoided the formation of more Friedel's salt and any scaling damage. Complete physical deterioration is the feature of damage in deteriorated samples in $CaCl_2$ solution. The specimens that experienced deterioration in the $CaCl_2$ exposure were seen to have network of microcracks under the microscope (Fig. 5.18). The concrete might have some micro-cracks prior to the F/T cycles but not in a form of network as observed in SEM. It refers that the damage in these specimens occurred due to physical damage resulted by repetitive F/T cycles.

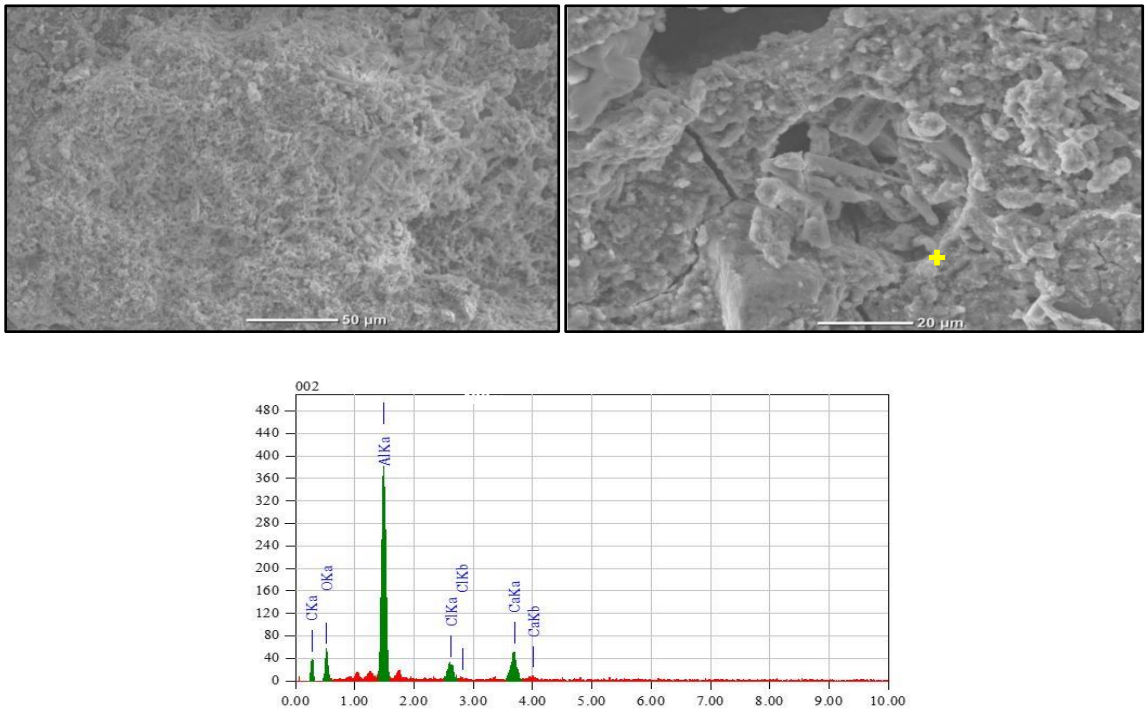

Figure 5.17: SEM micrographs and associated EDX spectra of fracture piece from GU specimen in $CaCl_2$ showingtraces of Friedel's salt.

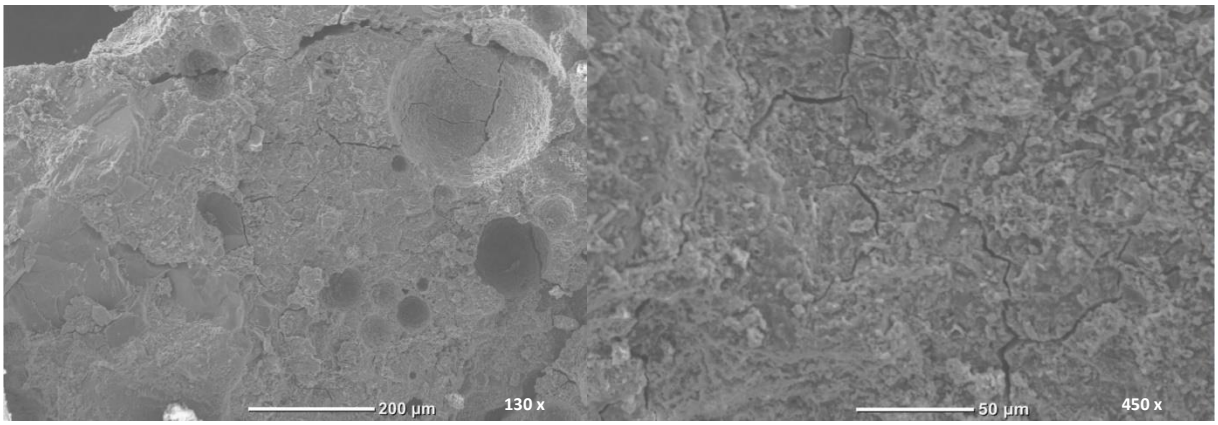

Figure 5.18: SEM micrographs showing micro-cracks of GU specimen in the $CaCl_2$ solution.

6. Summary, Conclusions and Recommendations

6.1. Summary

This thesis focused on evaluating concrete pavement sections (regional roads and residential streets) exposed to different winter treatments (type, rate and application [direct/indirect] of de-icing salts), which had been in service in wet and long freezing conditions between 15 and 20 years. The study presents the results of an evaluation for the condition of these concrete pavements through macro and micro scale analyses. In addition to the filed study, an experimental program was conducted to evaluate the effects of de-icing salts, various dosages of supplementary cementitious materials (SCMs) (fly ash and nanosilica) in concrete exposed to freeze-thaw (F/T) conditions. The assessment criteria were based on physical properties (physical penetrability, visual inspection, mass loss, length change and relative dynamic modulus of elasticity). In addition, the alteration of microstructure was examined by mineralogical, thermal and microscopy studies.

6.2. Conclusions for the Field Study

This study involved the evaluation of joints in pavement sections (regional roads and residential streets) exposed to different winter conditions (direct/indirect de-icing salts). The following conclusions can be drawn from the results of this investigation:

- Cores extracted from the regional roads exhibited higher rates of absorption and penetrability. Microstructural analysis disclosed that these cores had high intensity of micro-cracking and the majority of air voids were filled with secondary depositions. Also, the direct application of de-icing salts in the regional roads further enhanced the degree of saturation at joints.

- The forensic evaluation herein suggests that the principal reason for the deterioration of concrete pavement in regional roads appears to be related F/T damage, as a result of inadequate air-void system due to gradual in-filling of voids with secondary depositions (mostly ettringite).
- Residential streets, which were indirectly exposed to de-icing salts, had reduced absorption and penetrability, due to homogenous microstructure that were free of micro-cracks. Cores from residential streets showed incidental occurrences of secondary depositions partially in-filling air voids; however, this had an insignificant effect on the quality of air-void parameters, and thus these pavements maintained high resistance to F/T cycles.
- Irrespective of the application of de-icing salts, the pavement cross slope and drainage system played a significant role in improving the performance of joints in the residential streets by preventing them from critical saturation compared to that in regional roads which continued to entrap solutions long after wetting events. The proper design and frequent maintenance of the drainage system in residential streets would extend the service life of concrete pavement in such areas and mitigate serviceability issues. Therefore, frequent inspection of the drainage system needs to be a key component of the maintenance plan of concrete pavements.

6.3. Conclusions for the Laboratory Study

This study showed the efficient concrete mixture designs incorporating various dosages of GU cement, PLC, fly ash and nanoparticles (nano-modified fly ash concrete) for concrete pavements exposed to the most widely used chloride-based de-icing salts under F/T exposure. The following conclusions can be drawn:

- The overall trends from the F/T exposure indicate that the aggression of solutions, in an ascending order, is NaCl, $MgCl_2$, and $CaCl_2$. Generally, the results indicate that NaCl is not aggressive salt with respect to physical/chemical degradation of concrete, as no features of damage were detected up to 600 F/T cycles. Comparatively, the reference specimens (GU) and the binary binder containing 20% fly ash exposed to $MgCl_2$ or $CaCl_2$ solutions suffered significant surface scaling/damage.
- Compared to the control (GU) binder, the incorporation of 30% fly ash in concrete improved its resistance to F/T damage for all de-icing salt solutions due to reduced solution uptake and amount of portlandite (improved physical and chemical resistances). This trend was magnified by using an ultrafine pozzolan 'nanosilica' as no single mixture made with binary or ternary binders comprising nanosilica showed any features of damage up to the end of the exposure (600 cycles).
- The overall performance of PLC concrete was comparable and in some cases (single binder) better than the GU mixtures to resist the F/T damage. This might be ascribed to the improved physical resistance due to the higher fineness of the PLC (460 m^2/kg) in comparison to the GU cement (390 m^2/kg), which can improve the hydration process and microstructural evolution of concrete.

6.4. Recommendations for Future Work

The outcome of this study and the discussion presented here provides useful insights to extend further work in this area. The future recommended directions related to this research are as follows:

- Nano-modified fly ash mixtures showed the potential for allowing transportation agencies to control fresh and/or hardened properties by adjusting the proportions of ingredients,

especially for mixtures containing high volume of fly ash, and improved its resistance to F/T action. In this context, its field performance needs to be documented, which is recommended for future work.

- A combined salt (e.g. $MgCl_2$+$CaCl_2$) solution, which simulates a synergistic maintenance and protective strategy in winter for concrete pavements and bridges, should be considered for future work.
- More research is needed in the synergistic effects of environmental conditions (combined exposure of freezing-thawing and wetting-drying) to determine the effects of various combined exposures on concrete pavements and to understand the key mechanisms behind the deterioration of concrete pavement.

7. References

ACI (American Concrete Institute) Committee. (2016). "Guide to durable concrete." ACI 201.2R. Farmington Hills, MI.

American Concrete Pavement Association. (2002). "Life cycle cost analysis: a guide for comparing alternate pavement designs." Building Sustainable Highways in Canada. http://www.cement.ca/

Arribas-Colón, M., Radliński, M., Olek, J., and Whiting, N. (2012). "Investigation of premature distress around joints in PCC pavements: Parts I & II." Joint Transportation Research Program, Indiana Department of Transportation and Purdue University, West Lafayette, Indiana.

Arya, C., Buenfeld, N. R., & Newman, J. B. (1990). "Factors influencing chloride-binding in concrete." Cement and Concrete research, 20(2), 291-300.

ASTM C150. (2016). "Standard Specification for Portland Cement." ASTM International, West Conshohocken, PA, USA.

ASTM C192. (2015). "Standard Practice for Making and Curing Concrete Test Specimens in the Laboratory." ASTM International, West Conshohocken, PA, USA.

ASTM C215. (2014). "Standard test method for fundamental transverse, longitudinal, and torsional resonant frequencies of concrete specimens." ASTM International, West Conshohocken, PA, USA.

ASTM C233. (2014) "Standard Test Method for Air-Entraining Admixtures for Concrete." *ASTM International*, West Conshohocken, PA, 04.02.

ASTM C494. (2015). "Standard Specification for Chemical Admixtures for Concrete." ASTM International, West Conshohocken, PA, USA.

ASTM C666. (2015). "Standard test method for resistance of concrete to rapid freezing and thawing." West Conshohocken, PA, USA.

ASTM C1012. (2013). "Standard test method for length change of hydraulic-cement mortars exposed to a sulfate solution." ASTM International, West Conshohocken, PA, USA.

ASTM C1157. (2011). “Standard Performance Specification for Hydraulic Cement.” ASTM International, West Conshohocken, PA, USA.

Bautista, F. E., and Basheer, I. (2008). “Jointed Plain Concrete Pavement (JPCP) Preservation and Rehabilitation Design Guide.” California Department of Transportation.

Bassuoni, M.T., Nehdi, M.L., and Greenough, T.R. (2006). “Enhancing the reliability of evaluating chloride ingress in concrete using the ASTM C 1202 rapid chloride penetrability test.” Journal of ASTM International, 3(3), 13.

Bhatti, M. A., Barlow, J. A., and Stoner, J. W. (1996). "Modeling damage to rigid pavements caused by subgrade pumping," Journal of transportation engineering, 122 (1), 12-21.

Bianchini, A. (2013). "Evaluation of temperature-induced curling in concrete slabs using deflection difference analysis." Journal of Transportation Engineering, 139 (2), 130-137.

Brown, M.E. (Ed.). (1998). Handbook of thermal analysis and calorimetry, Amsterdam, Netherlands.

Brown, P. W., and Doerr, A. (2000). “Chemical changes in concrete due to the ingress of aggressive species.” Cement and Concrete Research, 30(3), 411-418.

Carde, C., & Francois, R. (1999). “Modelling the loss of strength and porosity increase due to the leaching of cement pastes.” Cement and Concrete Composites, 21(3), 181-188.

Chatterji, S., and Gudmundsson, H. (1977). “Characterization of entrained air bubble systems in concrete by means of an image analysing microscope.” Cement andConcrete Research, 7(4), 423-428.

City of Winnipeg. (2011). “Policy on snow clearing and ice control.” http://winnipeg.ca/publicworks/snow/snowClearing/snowClearingPolicy.stm#StreetPriorities (Feb. 1, 2017).

Cody, R. D., Spry, P. G., Cody, A. M., and Gan, G. L. (1994). “The role of magnesium in concrete deterioration.” Department of Geological and Atmospheric Sciences, Iowa State University.

Cody, R. D., Cody, A. M., Spry, P. G., and Gan, G. L. (1996). "Experimental deterioration of highway concrete by chloride de-icing salts." Environmental & Engineering Geoscience, 2 (4), 575-588.

Collepardi, M., Coppola, L., and Pistolesi, C. (1994). "Durability of Concrete Structures Exposed to $CaCl_2$ Based De-icing Salts." ACI Special Publications, 145, 107-107.

CSA (Canadian Standards Association). (2013). "Cementitious materials for use in concrete." CAN/CSA-A3001, Mississauga, Ontario, Canada.

CSA (Canadian Standards Association). (2014). "Concrete materials and methods of concrete construction/test methods and standard practices for concrete." CSA-A23.1/A23.2, Mississauga, Ontario, Canada.

Darwin, D., Browning, J., Gong, L., and Hughes., S. R. (2008). "Effects of De-icers on Concrete Deterioration." ACI Materials Journal, 105(6), 622-627.

Delagrave, A., Marchand, J., Ollivier, J. P., Julien, S., &Hazrati, K. (1997). "Chloride binding capacity of various hydrated cement paste systems." Advanced cement based materials, 6(1), 28-35.

Detwiler, R.J., and Powers-Couche, L.J. (1999). "Effects of sulfates in concrete on their resistance to freezing and thawing." ACI Special Publication 177-16, 219-247.

Detwiler, R. J., Nagi, M. A., and Bhattacharja, S. (2001). "Identifying combinations of materials that lead to premature deterioration in concrete pavements." Seventh International Conference on Concrete Pavements, The Use of Concrete in Developing Long-Lasting Pavement Solutions for the 21st Century. 1.

Famy, C., and Taylor, H.F.W. (2001). "Ettringite in hydration of portland cement concrete and its occurrence in mature concretes." ACI Materials Journal, 98(4), 350-356.

Fang, Y. F. (2001). "Environmental Influences on Warping and Curling of PCC Pavement." Seventh International Conference on Concrete Pavements, The Use of Concrete in Developing Long-Lasting Pavement Solutions for the 21st Century, 1.

Farnam, Y., Dick, S., Wiese, A., Davis, J., Bentz, D., & Weiss, J. (2015). "The influence of calcium chloride deicing salt on phase changes and damage development in cementitious materials." Cement and Concrete Composites,64, 1-15.

Farnam, Y., Wiese, A., Bentz, D., Davis, J., & Weiss, J. (2015). "Damage development in cementitious materials exposed to magnesium chloride de-icing salt." Construction and Building Materials,93, 384-392.

Gulati, S. T., and Hagy, H. E. (1982). "Analysis and Measurement of Glue-Spall Stresses in Glass-Epoxy Bonds." Journal of the American Ceramic Society, 65 (1), 1-5.

Hall C. (1989). "Water sorptivity of mortars and concretes: A review." Magazine ofConcrete Research, 41(14), 51-61.

Hall, K., Dawood, D., Vanikar, S., Tally, R., Cackler, J.T., Correa, A., Deem, P., Duit, J., Geary, G., Gisi, A., Hanna, A., Kosmatka, S., Rasmussen, R., Tayabji, S., and Voigt, G. (2007). "Long-life concrete pavements in Europe and Canada." Federal Highway Administration. http://international.fhwa.dot.gov/.

Gabrisova, A., Havlica, J., &Sahu, S. (1991). "Stability of calcium sulphoaluminate hydrates in water solutions with various pH values." Cement and Concrete Research, 21(6), 1023-1027.

Heath, A. C., Roesler, J. R., & Harvey, J. T. (2003). "Modeling longitudinal, corner and transverse cracking in jointed concrete pavements." International Journal of Pavement Engineering, 4(1), 51-58.

Helmuth, R. A. (1960). "Discussion of the paper "Frost Action in Concrete." Proc. 4th Int. Cong. Chemistry of Cement, NBS Monog 43,829-833.

Hoffmann, D. W. (1984). "Changes in structure and chemistry of cement mortars stressed by a sodium chloride solution." Cement and Concrete Research,14(1), 49-56.

Holt, A., Sullivan, S., and Hein, D.K. (2011). "Life cycle cost analysis of municipal pavements in Southern and Eastern Ontario." In Proceedings of the 2011 Annual Conference of the Transportation Association of Canada, Edmonton, Alberta, Canada.

Hossain, S., Fu, L., & Lu, C. Y. (2014). "De-icing Performance of Road Salt: Modeling and Applications." Transportation Research Record: Journal of the Transportation Research Board, 2440, 76-84.

Jain, J. A., Janusz, A. E., Olek, J., &Jozwiak-Niedzwiedzka, D. (2011)."Physico-chemical Changes in Plain and Fly Ash Modified Concretes Exposed to Different Deicing Chemicals," Proc., 13th International Congress on Chemistry of Cement.

Jain, J., Olek, J., Janusz, A., and Jozwiak-Niedzwiedzka, D. (2012). "Effects of deicing salt solutions on physical properties of pavement concretes." Transportation Research Record, 2290, 69-75.

Jones, W., Farnam, Y., Imbrock, P., Spiro, J., Villani, C., Olek, J., & Weiss, W. J. (2013). "An overview of joint deterioration in concrete pavement: Mechanisms, solution properties, and sealers."

Kang, Y., Hansen, W., and Borgnakke, C. (2012). "Effect of air-void system on frost expansion of highway concrete exposed to de-icer salt." International Journal of Pavement Engineering, 13(3), 259-266.

Kelting, D. L., and Laxson, C. L. (2010). "Review of Effects and Costs of Road De-icing with Recommendations for Winter Road Management in the Adirondack Park." Adirondack Watershed Institute, 34.

Kerr, A. D., and Dallis Jr., W. A. (1985). "Blowup of concrete pavements." Journal of transportation engineering, 111(1), 33-53.

Koubaa, A., and Snyder, M. B. (2001). "Assessing frost resistance of concrete aggregates in Minnesota." Journal of cold regions engineering, 15(4), 187-210.

Lee, H., Cody, R. D., Cody, A. M., & Spry, P. G. (2000). "Effects of various deicing chemicals on pavement concrete deterioration." Mid-Continente Transportation Symposium Proceedings.

Li, W., Pour-Ghaz, M., Castro, J., & Weiss, J. (2011). "Water absorption and critical degree of saturation relating to freeze-thaw damage in concrete pavement joints." Journal of Materials in Civil Engineering, 24(3), 299-307.

Litvan, G. G. (1976). "Frost action in cement in the presence of de-icers." Cement and Concrete Research,6(3), 351-356.

Mather, B. (2001). "Crystal growth in entrained air voids." Concrete International, 23(5), 35-36.

Marchand, EJ. J., and Pigeon, M. (1994). "De-icer Salt Scaling Deterioration--An Overview." Special Publication,145, 1-46.

Marchand, J., Pigeon, M., Bager, D., &Talbot, C. (1999). "Influence of chloride solution concentration on de-icer salt scaling deterioration of concrete." ACI Materials Journal, 96, 429-435.

Mehta, P. K., and Monteiro, P. (2014). “Concrete: Microstructure, properties, and materials.” McGraw-Hill, San Francisco, USA.

Miller, J. S., and Bellinger, W. Y. (2003). “Distress Identification Manual for the Long-Term Pavement Performance Program.” Federal Highway Administration, Fourth edition, 153.

Montgomery, D.C. (2014). Design and analysis of experiments, John Wiley and Sons, New York, USA.

Nicholson, K. W., and Branson, J. R. (1999). “Factors Affecting Resuspension by Road Traffic.”The Science of the Total Environment, 93, 349-358.

Nixon, P. J., Page, C. L., Canham, I., and Bollinghaus, R. (1988). "Influence of sodium chloride on alkali-silica reaction." Advances in cement research, 1(2), 99-106.

Olek, J., M. Radlinski, and Arribas, M. (2007). “Premature Deterioration of Joints in Selected Indiana Portland Cement Concrete Pavements.” Proceedings of the XXIII Conference, 859–868.

Olek, J. (2013). “Durability of Plain and Fly Ash Concretes Exposed to De-icing Chemicals.” Proceedings of the Third International Conference on Sustainable Construction Materials and Technologies, Kyoto, Japan.

Ouyang, C., and Lane, O.J. (1999). “Effect of infilling of air voids by ettringite on resistance of concretes to freezing and thawing.” ACI Special Publication 177-16, 249-261.

Page, C. L., and Page, M. M. (2007). “Durability of Concrete and Cement Composites.” International Conference for Pavement, Cambridge, England.

Panchmatia, P., Olek, J., and Whiting, N. (2014). “Joint Deterioration in Concrete Pavements.” 4th International Conference on the Durability of Concrete Structures, Purdue University, West Lafayette, IN, USA.

Peterson, K., Julio-Betancourt, G., Sutter, L., Hooton, R. D., & Johnston, D. (2013). "Observations of chloride ingress and calcium oxychloride formation in laboratory concrete and mortar at 5° C." Cement and Concrete Research, 45, 79-90.

Powers, T.C., and Helmuth, R. A. (1953). "Theory of volume changes in hardened portland-cement paste during freezing." Highway research board proceedings, 32.

Powers, T.C., and Willis, T. F. (1950). "The air requirement of frost resistant concrete," Highway Research Board Proceedings, 29.\

Public Works Department, City of Winnipeg D3310. (2014). “Portland Cement Concrete Pavement Works.” Standard Construction Specifications, Manitoba, Canada, 1053.

Radjy, F., Sellevoid, E. J., and Richards, C. W. (1972). "Effect of freezing on the dynamic mechanical response of hardened cement paste down to -60°C." Cement and Concrete Research, 2(6), 697-715.

Ramezanianpour, A. M., & Hooton, R. D. (2014). “A study on hydration, compressive strength and porosity of Portland-limestone cement mixes containing SCMs.” Cement and Concrete Composites, 51, 1-13.

Ranjaraju, P.R. (2002). “Investigating premature deterioration of a concrete highway.” Transportation Research Record, 1798, 1-7.

Rao, S., and Roesler, J. R. (2005). "Characterizing effective built-in curling from concrete pavement field measurements," Journal of Transportation Engineering, 131(4), 320-327.

Rösli, A., and Harnik, A. B. (1980). "Improving the durability of concrete to freezing and deicing salts." Durability of Building Materials and Components, ASTM International.

Said, A. M., Zeidan, M. S., Bassuoni, M.T., and Tian, Y. (2012). “Properties of Concrete Incorporating Nano-silica.” Construction and Building Materials, 36, 838-844.

Sanchez, F., and Sobolev, K. (2010). “Nanotechnology in Concrete – a Review.” Construction and Building Materials, 24(11), 2060-2071.

Santagata, M. C., and Collepardi, M. (2000). "The effect of CMA de-icers on concrete properties." Cement and concrete research,30 (9), 1389-1394.

Sargious, M. (1975). “Pavements and Surfacing for Highways and Airports.” John Wiley and Sons, New York, NY.

Scherer, G. W. (2004) “Stress from Crystallization of Salt.” Cement and Concrete Research, 34(9), 1613-1624.

Schwartz D, D. R. (1987) “D-Cracking of Concrete Pavements”, National Cooperative Highway Research Program, Synthesis of Highway Practice, 38p.

Setzer, M. J. (2001). "Micro-ice-lens formation in porous solid." Journal of colloid and interface science, 243(1), 193-201.

Shahin, M. Y. (2005). "Pavement management for airports, roads, and parking lots." New York: Springer, 501.

Shi, X., Fay, L., Peterson, M. M., & Yang, Z. (2010). "Freeze–thaw damage and chemical change of a portland cement concrete in the presence of diluted de-icers." Materials and Structures, 43 (7), 933-946.

Shi, X., Fay, L., Peterson, M. M., Berry, M., & Mooney, M. (2011). "A FESEM/EDX investigation into how continuous de-icer exposure affects the chemistry of Portland cement concrete." Construction and building materials, *25*(2), 957-966.

Skalny, J., Marchand, J., and Odler, I. (2002). "Sulfate attack on concrete." Spon Press, London, UK.

Stark, J., and Bollmann, K. (1999). "Laboratory and field examinations of ettringite formation in pavement concrete." ACI Special Publication 177-16, 183-191.

Sumsion, E. S., & Guthrie, W. S. (2013). "Physical and Chemical Effects of De-icers on Concrete Pavement: Literature Review," (No. UT-13.09).

Sun, Z., and Scherer, G. W. (2010). "Effect of air voids on salt scaling and internal freezing." Cement and Concrete Research, 40(2), 260-270.

Sutter, L., Dam, T., Peterson, K., & Johnston, D. (2006). "Long-term effects of magnesium chloride and other concentrated salt solutions on pavement and structural portland cement concrete: Phase I results." Transportation Research Record: Journal of the Transportation Research Board, 1979, 60-68.

Sutter, L., Peterson, K., Julio-Betancourt, G., Hooton, D., Dam, T. V., & Smith, K. (2008). "The deleterious chemical effects of concentrated de-icing solutions on Portland cement concrete." Final Report for the South Dakota Department of Transportation.

Thaulow, N., and Sadananda, S. (2004). "Mechanism of concrete deterioration due to salt crystallization." Materials Characterization, 53 (2), 123-127.

Tiznobaik, M., and Bassuoni, M.T. (2017). "A test protocol for evaluating absorption of joints in concrete pavements." ASTM Journal of Testing and Evaluation, in press.

Taylor, P.C. (2011). "Preventing Joint Deterioration in Concrete Pavements: A Summary of Current Knowledge." National Concrete Pavement Technology Center, 18.

Valenza II J.J., and Scherer, G.W. (2005). "Mechanisms of salt scaling." Materials and Structures, 38, 479–488.

Valenza, J. J., & Scherer, G. W. (2006). "Mechanism for salt scaling." Journal of the American Ceramic Society, 89(4), 1161-1179.

Valenza II, J. J., and Scherer, G. W. (2007) "A Review of Salt Scaling: I. Phenomenology." Cement and Concrete Research, 37(7), 1007-1021.

Valenza II, J. J., and Scherer, G. W. (2007) "Mechanism for Salt Scaling of a Cementitious Surface." Materials and Structures, 40, 259-268.

Valenza II, J. J., and Scherer, G. W. (2007) "A Review of Salt Scaling: II. Mechanisms."Cement and Concrete Research, 37, 1022-1034.

Van Wijk, A. J., Larralde, J., Lovell, C. W., & Chen, W. F. (1989). "Pumping prediction model for highway concrete pavements." Journal of transportation engineering, 115(2), 161-175.

Wang, K., Nelson, D.E., and Nixon, W.A. (2006). "Damaging effects of deicing chemicals on concrete materials." Cement and Concrete Composites, 28(2), 173-188.

Wardeh, G., Mohamed, M. A., and Ghorbel, E. (2011). "Analysis of concrete internal deterioration due to frost action." Journal of Building Physics, 35(1), 54-82.

Wu, Z., Shi, C., Gao, P., Wang, D., & Cao, Z. (2014). "Effects of De-icing Salts on the Scaling Resistance of concrete." Journal of Materials in Civil Engineering, 27(5), 04014160.

Yang, W. C., Ge, Y., Zhang, B. S., and Yuan, J. (2011). "Effect of Saturation Degree on Concrete Deterioration Due to Freeze-Thaw Action." Key Engineering Materials, 477, 404-408.

Yener, E., and Hinislioğlu, S. (2011). "The effects of silica fume and fly ash on the scaling resistance and flexural strength of pavement concretes." Road Materials and Pavement Design,12(1), 177-194.

Zalocha, D., and Kasperkiewicz, J. (2005). “Estimation of the structure of air entrained concrete using a flatbed scanner.” Cement and Concrete Research, 35(10), 2041-2046.

Appendix A: Field Work

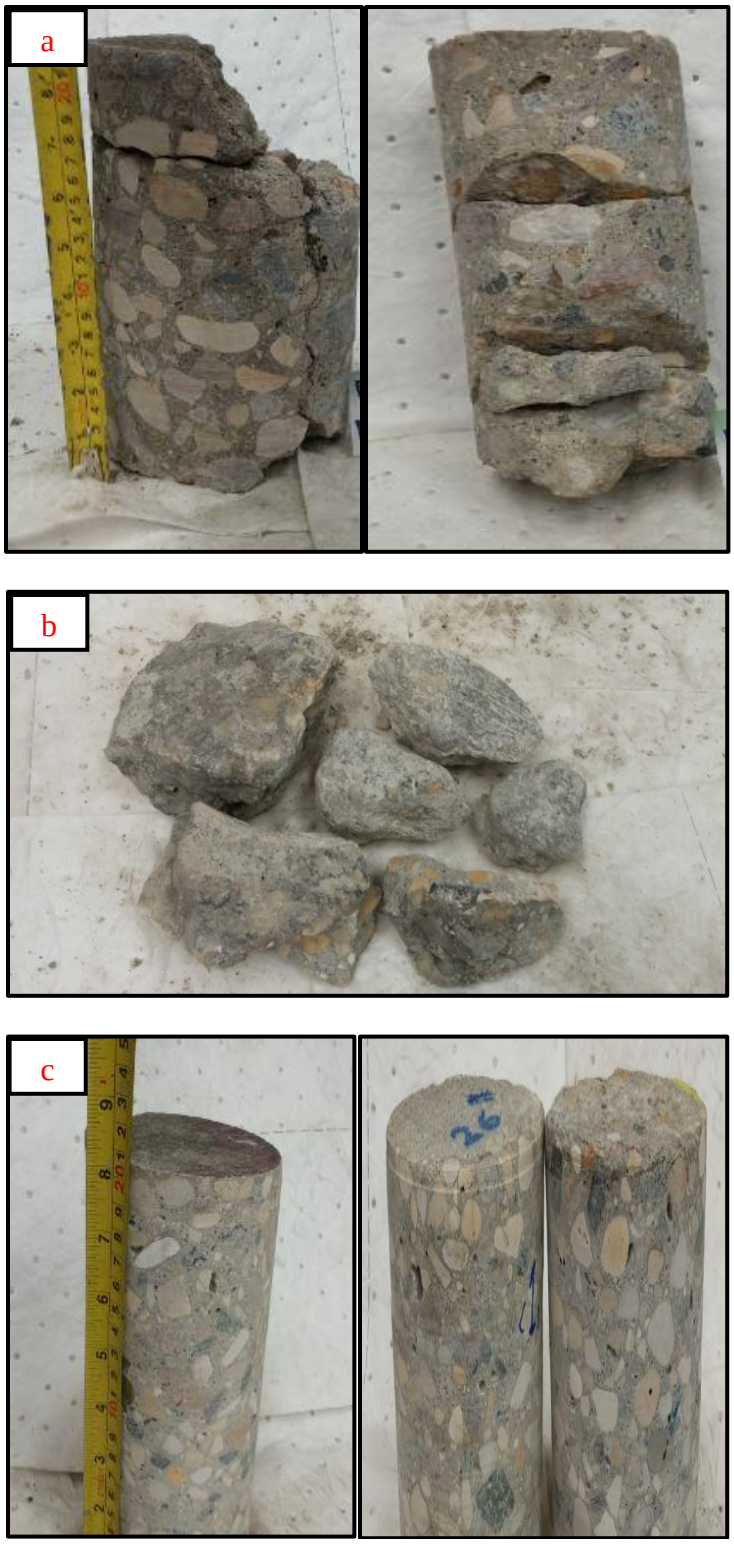

Figure A.1: Collected (a) deteriorated (b) crumbled and (c) undeteriorated cores from the field

Appendix B: Laboratory Work

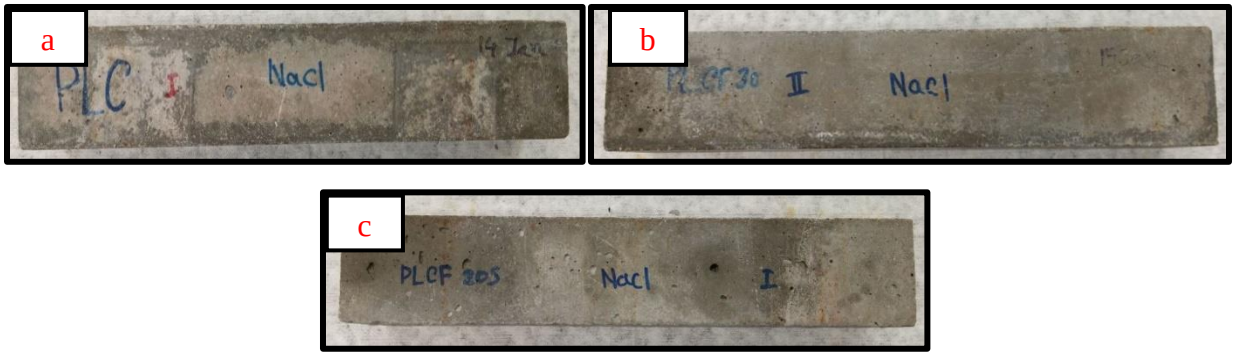

Figure B.1: Intact specimens exposed to the NaCl solution after 600 F/T cycles: (a) single (PLC) (b) binary (GUF30), and (c) ternary (GUF20S) binders.

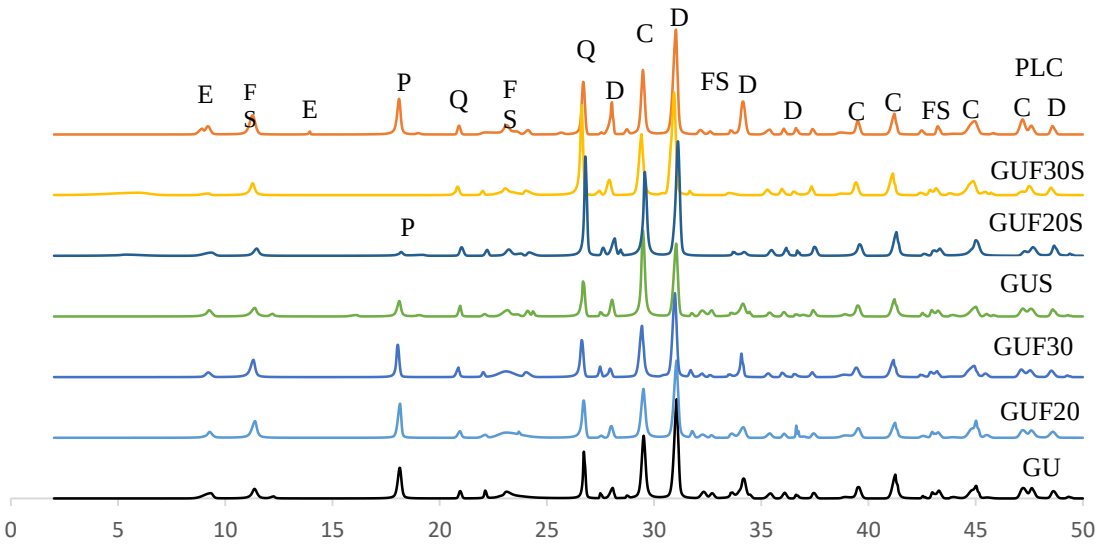

Figure B.2: XRD patterns of specimens exposed to the NaCl solution. (Note: E= ettringite, FS= Friedel's salt, P= portlandite, Q= quartz, D= dolomite, C= calcite)

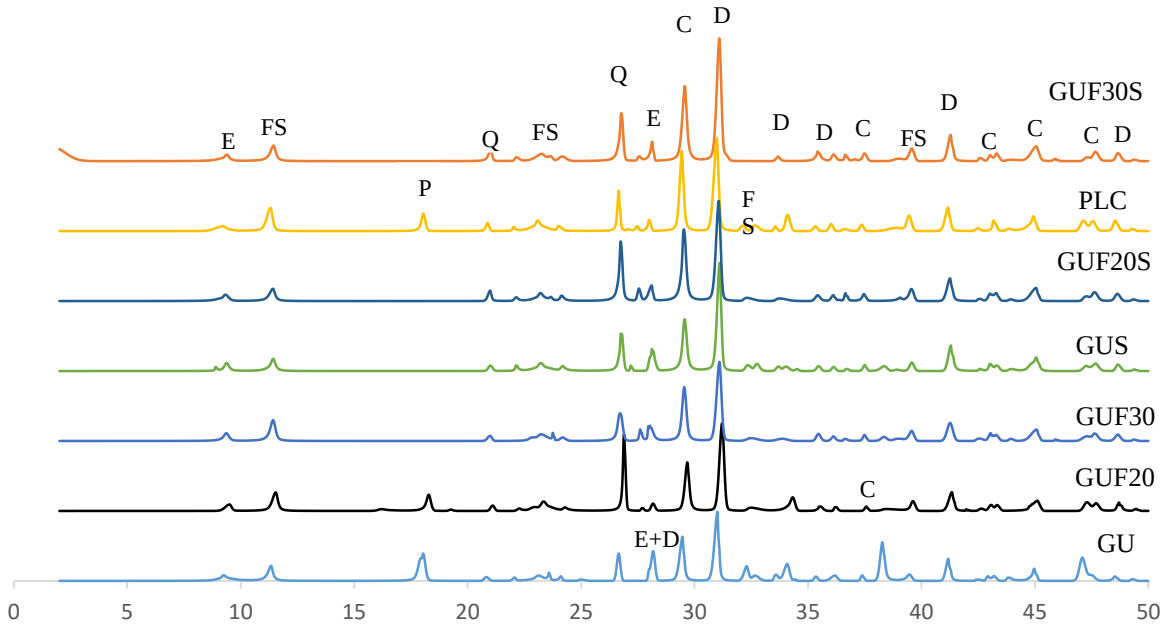

Figure B.3: XRD patterns of specimens exposed to the $CaCl_2$ solution. (Note: E= ettringite, FS= Friedel's salt, P= portlandite, Q= quartz, D= dolomite, C= calcite)